

Probabilistic seismic hazard in the San Francisco Bay area based on a simplified viscoelastic-cycle model of fault interactions

Fred F. Pollitz and David Schwartz

U.S. Geological Survey, Menlo Park, California

F. F. Pollitz, U.S. Geological Survey, 345 Middlefield Rd., MS 977, Menlo Park, CA 94025

D. Schwartz, U.S. Geological Survey, 345 Middlefield Rd., MS 977, Menlo Park, CA 94025

Abstract.

We construct a viscoelastic-cycle model of plate boundary deformation that includes the effect of time-dependent interseismic strain accumulation, coseismic strain release, and viscoelastic relaxation of the substrate beneath the seismogenic crust. For a given fault system, time-averaged stress changes at any point (not on a fault) are constrained to zero, i.e., kinematic consistency is enforced for the fault system. The dates of last rupture, mean recurrence times, and the slip distributions of the (assumed) repeating ruptures are key inputs into the viscoelastic cycle model. This simple formulation allows construction of stress evolution at all points in the plate boundary zone for purposes of probabilistic seismic hazard analysis (PSHA). Stress evolution is combined with a Coulomb failure stress threshold at representative points on the fault segments to estimate the times of their respective future ruptures. In our PSHA we consider uncertainties in a four-dimensional parameter space: the rupture periodicities, slip distributions, time of last earthquake (for pre-historic ruptures) and Coulomb failure stress thresholds. We apply this methodology to the San Francisco Bay region using a recently-determined fault chronology of area faults. Assuming single-segment rupture scenarios, we find that future rupture probabilities of area faults in the coming decades are the highest for the southern Hayward, Rodgers Creek, and northern Calaveras faults. This conclusion is qualitatively similar to that of *Working Group on California Earthquake Probabilities* [2003], but the probabilities derived here are significantly higher. Given that fault rupture prob-

abilities are highly model dependent, no single model should be used to assess to time-dependent rupture probabilities. We suggest that several models, including the present one, be used in a comprehensive PSHA methodology, as was done in *Working Group on California Earthquake Probabilities* [2003].

1. Introduction

Approaches in probabilistic seismic hazard analysis (PSHA) have up to the present time been primarily statistical, i.e., based on Poissonian or other mathematical probability density functions for future rupture forecasts. This has been because of difficulties in identifying all important faults in a region combined with the large uncertainties in faulting histories for known faults, making deterministic approaches problematic. Any deterministic approach must use an idealized model of fault system behavior. Since fault systems are complex, even simple models of fault system behavior yield chaotic behavior, but such models carry the advantage of representing this behavior with only a few controlling parameters.

Where faulting histories are well-known, such as along the North Anatolian Fault Zone in northern Turkey, deterministic approaches have been introduced based on interaction probabilities in the joint framework of Coulomb stress failure theory and rate and state friction theory [Parsons, 2000]. The principle of an interaction probability is that past faulting history combined with estimated recurrence time(s) form the backbone of the deterministic component of the analysis, whereas mathematical functions representing aperiodicity and/or rate and state friction theory contain the random component of the analysis. In northern California, *Working Group on California Earthquake Probabilities* [2003] made an attempt to include interaction probabilities by considering the coseismic stress change imparted by the 1906 San Francisco earthquake [Thatcher *et al.*, 1997] and the consequent impact on time-to-failure of neighboring fault segments.

The coseismic stress change associated with a past major earthquake is an important component of the seismic cycle, but postseismic motions following such earthquakes are an equally important component. Recently, *Michael* [2005] and *Hardebeck* [2004] introduced formalisms for incorporating coseismic and/or postseismic stresses in PSHA. *Michael* [2005] considered the special case of faulting cycles with viscoelastic postseismic relaxation represented with a single decaying exponential function. He superimposed postseismic relaxation on background loading and a Brownian Passage Time (BPT) model of random stresses to estimate the impact of postseismic stresses on future event probabilities. The approach of *Hardebeck* [2004] considers first the future event probability distributions in the absence of stress perturbations and the consequent modification of these probability distributions from inclusion of these perturbations. Hardebeck's approach is more general in the sense that the random component of the deformation process is not explicitly specified. Her approach can accommodate the deterministic components of the strain accumulation and coseismic and postseismic stress processes without appeal to an underlying physical model. It can be implemented for any physical failure model, as long as one can quantify the change in time to failure as a function of stress change; her approach employs the rate-and-state time-to-failure equations for this purpose.

Here our aim is to connect simple physical models with the "background" strain accumulation and coseismic and postseismic processes, as a means of gaining a more complete understanding of the deterministic components of the deformation processes that occur during a seismic cycle. Linear viscoelastic coupling models [*Savage and Prescott*, 1978; *Pollitz*, 2001; *Pollitz*, 2003] are used for this purpose. When combined with a Coulomb

failure stress threshold, the stress evolution allows formal estimation of the times of future rupture of the faults in the plate boundary system.

We apply this approach to the faults of the San Francisco Bay region (SFBR). We construct an earthquake history for the region based on the known times of historic events, estimated times of historic events, and estimated repeat times. We then proceed to consider uncertainties in the system and propagate their effects through the stress evolution to derive conditional probability distributions for future ruptures. The evaluation of rupture probabilities in this study is not as comprehensive as that of of *Working Group on California Earthquake Probabilities* [2003]. However, our re-evaluation is based on a different approach and, more importantly, exploits updated earthquake chronologies on several Bay-area faults, particularly on the southern Hayward fault where the mean recurrence interval is more tightly constrained. As a result, resulting earthquake probabilities for the Hayward fault and other faults are significantly higher than those derived by *Working Group on California Earthquake Probabilities* [2003].

2. Stress evolution in a viscoelastic coupling model

We assume that a definite volume contains a number of faults, each rupturing periodically with uniform slip and recurrence interval (which may differ from fault to fault). Stress accumulated at point \mathbf{r} up to time t is a combination of accumulated coseismic stress, postseismic stress, and background loading:

$$\sigma(\mathbf{r}, t) = \sigma(\mathbf{r}, t_0) + \sum_i [\sigma_{\text{co}}^{(i)}(\mathbf{r}, t)|_{t_0}^t] + \sum_i [\sigma_{\text{ps}}^{(i)}(\mathbf{r}, t)|_{t_0}^t] + \dot{\sigma}_{\text{load}}(\mathbf{r}) \times (t - t_0) \quad (1)$$

where accumulated coseismic and postseismic stress in a time interval (t_1, t_2) are:

$$\sigma_{\text{co}}^{(i)}(\mathbf{r}, t)|_{t_1}^{t_2} = \sum_{n=0}^{\infty} \sum_{jk} \int m_{jk}^{(i)}(\mathbf{r}_0) \Psi_{jk}(\mathbf{r}, \mathbf{r}_0, 0^+) [H(t - t_i + nT_i)|_{t_1}^{t_2}] d^3\mathbf{r}_0 \quad (2)$$

$$\sigma_{ps}^{(i)}(\mathbf{r}, t)|_{t_1}^{t_2} = \sum_{n=0}^{\infty} \sum_{jk} \int m_{jk}^{(i)}(\mathbf{r}_0) \{ [\Psi_{jk}(\mathbf{r}, \mathbf{r}_0, t - t_i + nT_i) - \Psi_{jk}(\mathbf{r}, \mathbf{r}_0, 0^+)] \times H(t - t_i + nT_i) \}|_{t_1}^{t_2} d^3\mathbf{r}_0 \quad (3)$$

In equations (1)-(3):

t_i = time of last event on fault i .

T_i = recurrence interval on fault i .

$m_{jk}^{(i)}(\mathbf{r}_0)$ = jk moment tensor density component of repeating source at point \mathbf{r}_0 on fault i .

$\Psi_{jk}(\mathbf{r}, \mathbf{r}_0, t)$ = Greens function for accumulated stress at point \mathbf{r} and time t in the viscoelastic system arising from unit jk -component moment tensor source applied at point \mathbf{r}_0 and time 0. The use of linear viscoelasticity allows G to be defined independently of the stress state, so that there is no non-linear interaction between the loading and postseismic stress fields. The stress can be a linear combination of stress tensor components evaluated at \mathbf{r} , e.g., the Coulomb stress function.

$H(t)$ = Heaveside step function.

$\dot{\sigma}_{load}$ = background loading rate.

An earthquake cycle for a particular fault $\#i$ refers to the net deformation occurring over an entire recurrence interval T_i , i.e. the totality of loading and coseismic and postseismic deformation. A natural choice for the loading rate is

$$\dot{\sigma}_{load}(\mathbf{r}) = -\left\{ \sum_i \left[\frac{1}{T_i} \sigma_{co}^{(i)}(\mathbf{r}, t)|_{0^+}^{T_i+0^+} \right] + \langle \dot{\sigma}_{ps}^{(i)}(\mathbf{r}, t) \rangle \right\} \quad (4)$$

where [Pollitz, 2003]

$$\langle \dot{\sigma}_{ps}^{(i)}(\mathbf{r}, t) \rangle = \frac{1}{T_i} \sum_{jk} \int m_{jk}^{(i)}(\mathbf{r}_0) \{ [\Psi_{jk}(\mathbf{r}, \mathbf{r}_0, \infty) - \Psi_{jk}(\mathbf{r}, \mathbf{r}_0, 0^+)] \} d^3\mathbf{r}_0 \quad (5)$$

is the postseismic stress rate contributed by fault i averaged over many cycles. Eqn (4) states that the loading rate negates the summed coseismic and postseismic stress changes averaged over one complete cycle for every fault. A more physical interpretation is that the system is loaded by backslip imposed on a thin elastic plate, i.e. the mechanical state achieved in the limit of complete relaxation. This is fundamentally a consequence of: (1) zero long-term strength below the base of the elastic plate and (2) the summation of viscoelastic relaxation from an infinite series of past events (on a given fault) assumed to have occurred periodically.

Equations (3) and (5) lead to the identity

$$\sigma_{ps}^{(i)}(\mathbf{r}, t)|_t^{t+T_i} = T_i \langle \dot{\sigma}_{ps}^{(i)}(\mathbf{r}, t) \rangle \quad (6)$$

It follows from equations (1), (2), (4), and (6) that for a fault system associated with a single mean recurrence time T_i ,

$$E\{\sigma(\mathbf{r}, t + T_i)\} = E\{\sigma(\mathbf{r}, t)\} \quad (7)$$

where the notation $E\{\}$ denotes expectation value of the quantity in brackets. If we decompose $\sigma(\mathbf{r}, t)$ into the contributions from faults of various recurrence times, this leads to

$$\lim_{\Delta t \rightarrow \infty} \frac{E\{\sigma(\mathbf{r}, t + \Delta t) - \sigma(\mathbf{r}, t)\}}{\Delta t} = 0 \quad (8)$$

This implies that over sufficiently long time periods (i.e., $\Delta t \gg T_i$ for all i) the theoretical stress release equals accumulated stress at any point.

3. Meaning of background loading

3.1. Loading of a strictly localized shear zone

In a strike-slip faulting environment embedded in a thin-plate system, consider a plate tectonic velocity v_0 accommodated across a plate boundary zone of width W . This corresponds to loading through horizontally transmitted shear, with all deformation strictly localized within the shear zone which is assumed bounded by rigid material. Choosing σ to be the horizontal shear stress on a vertical plane parallel to the plate boundary, we have a shear strain rate of $-(1/2)v_0/W$ and hence

$$\dot{\sigma}_{load}(\mathbf{r}) = -\mu \frac{v_0}{W} \quad (9)$$

for $\mathbf{r} \in$ plate boundary zone, where μ is the shear modulus. In the *Savage and Prescott* [1978] two-dimensional (2D) viscoelastic system containing an infinitely long strike-slip fault that is entirely locked during the interseismic period, W is arbitrarily large and hence $\dot{\sigma}_{load} = 0$. This is easily rationalized in terms of the relationship given in eqn (4). The sum of coseismic and postseismic motions of an infinitely-long fault that penetrates the entire elastic layer reduces to block motion of one side of the fault with respect to the other, which is associated with zero net stress.

The case of finite W in a 2D strike-slip faulting environment was treated by *Pollitz* [2001]. In that case eqn (9) yields a non-trivial $\dot{\sigma}_{load}$. The relationship of eqn (4) is still valid, but in this case the compounded coseismic and postseismic deformation fields reduce to a simple shear stress that negates $\dot{\sigma}_{load}$ over the seismic cycle. For example, take the plate boundary edges to be at $x = 0$ and $x = W$ and consider a single strike-slip fault located at $x = \delta$; let the recurrence time be T . The net slip across the fault at the end of a cycle is $v_0 T$. If $u_y(x)$ denotes the fault-parallel displacement, then the displacement

field associated with loading over one cycle is

$$u_y(x) = (v_0 T) \left(1 - \frac{x}{W}\right) \quad (10)$$

and that associated with total coseismic and postseismic motions over one cycle is given by

$$u_y(x) = (v_0 T) \frac{x}{W} \quad x \in (0, \delta) \quad (11)$$

$$u_y(x) = (v_0 T) \left(\frac{x}{W} - 1\right) \quad x \in (\delta, W) \quad (12)$$

The total stress change in the elastic layer associated with coseismic and postseismic motions equals

$$\mu \frac{v_0}{W} T \quad (13)$$

i.e., $-\dot{\sigma}_{load} \times T$, which obeys eqn (4).

Eqn (9) for the loading rate in a plate boundary zone of width W also applies to a multi-fault system, including a three-dimensional distribution of faulting that includes a mixture of segments of finite length and creeping faults. However, the equality of stress release and stress accumulation over long time periods stated by equations (7) and (8) is valid only if eqn (4) is satisfied. This requires, in turn, that the fault system be kinematically self-consistent. For example, a right-lateral strike-slip fault system containing a right step must contain a zone of rifting along fault(s) at the right step which opens at the same rate as the strike-slip fault segments. Similarly, a long strike-slip fault may be composed of locked and creeping portions as long as the creep rate equals the long-term slip rate on the locked portions of that fault.

Note that creeping faults may be implemented in this framework by defining a set of faults with T_i vanishing small and $m_{jk}^{(i)}$ chosen such that

$$\lim_{T_i \rightarrow 0} m_{jk}^{(i)}(\mathbf{r}_0) / T_i \quad (14)$$

equals the rate of moment release density at point \mathbf{r}_0 . The formal contribution of creeping segments to the stress accumulation rate in eqn (1) is then accommodated through the $\sigma_{\infty}^{(i)}$ and $\sigma_{ps}^{(i)}$ terms rather than the $\dot{\sigma}_{load}$ term.

Although we do not explore the case of subduction loading in detail here, we note that equations (1) and (4) are equivalent to eqn (10) of *Savage* [1983] for the evolution of a viscoelastic system driven by subduction zone loading and stress release. As for the strike-slip case, eqn (7) implies a zero net stress change over one cycle (for example, for a single fault representing a convergent plate boundary); eqn (8) implies the same averaged over many cycles. There are alternative formulations for the loading of both strike-slip and convergent plate boundaries combined with cyclic stress release such that equations (7) and (8) are not satisfied [*Pollitz and Vergnolle*, 2006]. Such a formulation would imply the existence of areas where stress builds up from one cycle to the next, implying the eventual creation of new faults. However, we restrict attention to the case in which eqn (4) and hence equations (7) and (8) are all satisfied.

3.2. Loading of system with finite shear modulus

The form of $\dot{\sigma}_{load}$ in eqn (9) is a pathological case in which the material bounding the shear zone is perfectly rigid ($\mu = \infty$ for $x \leq 0$ and $x \geq W$), so that coseismic and postseismic perturbations are constrained to have zero displacements on the shear zone edges, i.e., $u_y(0) = u_y(W) = 0$. Equation (4), with the summed coseismic and postseismic

deformation given by equations (11) and (12), is satisfied with a non-trivial $\dot{\sigma}_{load}$ given by equation (9). However, any system with a finite shear modulus distribution in the Earth and which builds up zero net stress over a complete cycle should satisfy

$$\sum_i \left[\frac{1}{T_i} \sigma_{co}^{(i)}(\mathbf{r}, t) \Big|_{0^+}^{T_i+0^+} \right] + \langle \dot{\sigma}_{ps}^{(i)}(\mathbf{r}, t) \rangle = \sum_i \frac{1}{T_i} \sum_{jk} \int m_{jk}^{(i)}(\mathbf{r}_0) \Psi_{jk}(\mathbf{r}, \mathbf{r}_0, \infty) d^3\mathbf{r}_0 = 0 \quad (15)$$

where it is understood that the response function $\Psi_{jk}(\mathbf{r}, \mathbf{r}_0, \infty)$ is to be evaluated on a 3D Earth model. More precisely, it should satisfy the equations of quasi-static equilibrium on a 3D laterally heterogeneous Earth model with an earthquake source (i.e., Appendix A of *Pollitz, 2003*). Eqn (15) states that at points not located directly on a fault, the time-averaged completely relaxed response to all dislocation sources is zero, i.e., blocks bounded by the faults behave rigidly over the long term. From eqn (4) it follows that

$$\dot{\sigma}_{load}(\mathbf{r}) = 0 \quad (16)$$

is appropriate for an Earth rheology model with finite shear modulus distribution and characterized by viscoelastic coupling cycles that are associated with vanishingly small net stress change when averaged over a large number of cycles.

An example is illustrated in Figure 1a for the case of a right-lateral strike-slip fault with a right step, where motion is accommodated by rifting. If the strike-slip faults (segments #1 and 3) are infinitely long and all faults slip with identical slip rate ($\dot{s}_1 = \dot{s}_2 = \dot{s}_3$), then the two blocks behave rigidly, and eqns (15) and (16) are satisfied. If one or more of these conditions were not satisfied, then the blocks would not behave rigidly and $\dot{\sigma}_{load}(\mathbf{r})$ would be generally non-zero.

3.3. Rationalization of a system containing thrust fault(s)

Eqn (15) is meant to hold in a global sense. Its validity can be easily imagined for a system containing a single strike-slip fault that makes a great-circle circuit around the spherical Earth, or several parallel strike-slip faults that make small circles around the spherical Earth, or even a small-circle fault that has both right and left stepovers with zones of rifting or compression within the stepovers (e.g. Figure 1a). The kinematics of such a stepover are straightforward for a zone of plate creation with a rift geometry, but requires special consideration for a zone of plate destruction, e.g., a thrust fault system.

As an example, for the case of repeated rupture of a megathrust at a convergent plate boundary (Figure 1b), eqn (15) would fail in the upper plate if the only dislocation source were slip on the megathrust. However, if the downgoing plate is imagined as a moving conveyor belt that drags the upper plate with it during interseismic periods and releases the accumulated stress with periodic slip events, then the upper plate is on average undeformed and one would expect eqn (15) to be satisfied. This apparent paradox is explained by the fact that the downgoing plate must undergo permanent deformation over a complete earthquake cycle. The process of plate bending at outer rise, which transforms horizontal motions at distance into descending motions along the contact with the upper plate, results in secular stressing around the outer rise. This bending zone is illustrated schematically in Figure 1b). Thus eqn (15) would fail in the downgoing plate as well. A conceptual remedy is to divide the bending zone into an arbitrarily large number of small blocks, and impose a distribution of moment tensor density $m_{jk}(\mathbf{r}_0)$ at the block boundaries such that, in conjunction with the slip on the megathrust, the downgoing plate behaves as the conveyor belt described above while each microblock behaves rigidly. The

combined effect of slip on the megathrust and the distributed sources within the bending zone would allow eqn (15) to be satisfied in the upper plate.

4. Imposed kinematic self-consistency

Suppose that a collection of faults Ω_{known} , which defines fault geometry and slip sense, is specified together with fault history $\{t_i, T_i; i \in \Omega_{\text{known}}\}$. If $\dot{\sigma}_{\text{load}}$ is constrained to obey eqn (4), then eqn (15) will hold if and only if the prescribed set of faults is kinematically self-consistent. If fault geometries, recurrence intervals, etc. are provided by independent sources, or if the faulting geometry or history is simply incomplete, then this will not be the case. The thrust-faulting system given in section 3.3 is a good example: slip on the megathrust alone is not sufficient to satisfy eqn (15).

It is possible to impose kinematic self-consistency by defining a set Ω_{unknown} containing information about unknown fault geometry and history that is excluded by Ω_{known} . In principle, Ω_{unknown} could even contain revisions to several of the parameters contained in Ω_{known} . The purpose of introducing the set of unknown faults is to enable one to fulfill both eqn (4) and kinematic self-consistency (i.e., eqn (15) or (16)) simultaneously. Let

$$\Omega = \Omega_{\text{known}} \cup \Omega_{\text{unknown}} \quad (17)$$

be the complete set of faults that comprise a kinematically self-consistent model. We assume an Earth rheology with finite shear modulus distribution, so that eqn (16) applies and we thus suppose that Ω has been chosen such that

$$\begin{aligned}
 \dot{\sigma}_{load}(\mathbf{r}) &= -\left\{ \sum_{i \in \Omega} \left[\frac{1}{T_i} \sigma_{co}^{(i)}(\mathbf{r}, t) \Big|_{0^+}^{T_i+0^+} \right] + \langle \dot{\sigma}_{ps}^{(i)}(\mathbf{r}) \rangle \right\} \\
 &= -\left\{ \sum_{i \in \Omega_{known}} \left[\frac{1}{T_i} \sigma_{co}^{(i)}(\mathbf{r}, t) \Big|_{0^+}^{T_i+0^+} \right] + \langle \dot{\sigma}_{ps}^{(i)}(\mathbf{r}) \rangle \right\} \\
 &\quad - \left\{ \sum_{i \in \Omega_{unknown}} \left[\frac{1}{T_i} \sigma_{co}^{(i)}(\mathbf{r}, t) \Big|_{0^+}^{T_i+0^+} \right] + \langle \dot{\sigma}_{ps}^{(i)}(\mathbf{r}) \rangle \right\} = 0
 \end{aligned} \tag{18}$$

Eqn (1) reads

$$\begin{aligned}
 \sigma(\mathbf{r}, t) &= \sigma(\mathbf{r}, t_0) + \sum_{i \in \Omega_{known}} [\sigma_{co}^{(i)}(\mathbf{r}, t) \Big|_{t_0}^t] + \sum_{i \in \Omega_{known}} [\sigma_{ps}^{(i)}(\mathbf{r}, t) \Big|_{t_0}^t] \\
 &\quad + \sum_{i \in \Omega_{unknown}} [\sigma_{co}^{(i)}(\mathbf{r}, t) \Big|_{t_0}^t] + \sum_{i \in \Omega_{unknown}} [\sigma_{ps}^{(i)}(\mathbf{r}, t) \Big|_{t_0}^t] \\
 &\quad \quad \quad + \dot{\sigma}_{load}(\mathbf{r}) \times (t - t_0)
 \end{aligned} \tag{19}$$

Two classes of $\Omega_{unknown}$ allow kinematic self-consistency to be applied without any direct use of this set. In the first case, $\Omega_{unknown}$ contains creeping faults, which are characterized by eqn (14) for a countably infinite sequence of past "events" in the limit $T_i \rightarrow 0$. The stress evolution contributed by these faults is linear in time, i.e.,

$$\sum_{i \in \Omega_{unknown}} [\sigma_{co}^{(i)}(\mathbf{r}, t) \Big|_{t_0}^t] + \sum_{i \in \Omega_{unknown}} [\sigma_{ps}^{(i)}(\mathbf{r}, t) \Big|_{t_0}^t] \sim t - t_0 \tag{20}$$

Substituting eqn (18) into (19) and making use of eqn (6), it follows that the terms that arise from $\Omega_{unknown}$ cancel, so that (19) simplifies into

$$\begin{aligned}
 \sigma(\mathbf{r}, t) &= \sigma(\mathbf{r}, t_0) + \sum_{i \in \Omega_{known}} [\sigma_{co}^{(i)}(\mathbf{r}, t) \Big|_{t_0}^t] + \sum_{i \in \Omega_{known}} [\sigma_{ps}^{(i)}(\mathbf{r}, t) \Big|_{t_0}^t] \\
 &\quad \quad \quad + [\dot{\sigma}_{load}(\mathbf{r})] \Big|_{\Omega_{known}} \times (t - t_0)
 \end{aligned} \tag{21}$$

where

$$[\dot{\sigma}_{load}] \Big|_{\Omega_{known}}(\mathbf{r}) = -\left\{ \sum_{i \in \Omega_{known}} \left[\frac{1}{T_i} \sigma_{co}^{(i)}(\mathbf{r}, t) \Big|_{0^+}^{T_i+0^+} \right] + \langle \dot{\sigma}_{ps}^{(i)}(\mathbf{r}, t) \rangle \right\} \tag{22}$$

In the second case, we suppose that both coseismic offsets and postseismic relaxation from past events on the unknown faults are treated in a statistical sense such that the time of the last event t_i is considered to be a random variable that can take any value within the interval $(t - T_i, t)$ (i.e., *Pollitz, 2003*). In the sense of expectation value over the range of possible t_i , we then have

$$E\{\sigma_{\text{co}}^{(i)}(\mathbf{r}, t)|_{t_0}^t\} = \frac{t - t_0}{T_i} \sigma_{\text{co}}^{(i)}(\mathbf{r}, t)|_{0^+}^{T_i+0^+}$$

$$E\{\dot{\sigma}_{\text{ps}}^{(i)}(\mathbf{r}, t)\} = \langle \dot{\sigma}_{\text{ps}}^{(i)}(\mathbf{r}, t) \rangle \quad i \in \Omega_{\text{unknown}} \quad (23)$$

This results in eqn (20), which leads again to the result in equations (21) and (22). It is clear that a superposition of unknown faults of both types leads to the same results. Thus a combination of creeping and locked faults is available (to be appended to the known faults) to create a kinematically self-consistent model.

5. Application to San Francisco Bay region

5.1. Earthquake chronology

Referring to Figure 2 we define a 8-fault system consisting of the rupture zones of regional events that occurred over the past ~ 300 years: $M \sim 7$ (1700) Concord-Green Valley earthquake, a $M \sim 7$ (1705) Northern Hayward fault earthquake, a $M \sim 7.5$ (1720) event on the San Andreas fault (SAF) north of the Golden Gate, a $M \sim 7$ (1740) Rodgers Creek fault earthquake, a $M \sim 7$ (1760) Northern Calaveras fault earthquake, the $M \sim 7$ 1838 Peninsula earthquake, the $M=6.8$ 1868 Hayward fault earthquake [*Yu and Segall, 1996*], the $M=7.9$ 1906 San Francisco earthquake [*Thatcher et al., 1997*], and the $M=6.9$ 1989 Loma Prieta earthquake [*Marshall et al., 1991*]. Fault parameters associated with these ruptures are given in Tables 1 and 2. Where repeat times are uncertain (as they

are for most of the pre-historic ruptures) they are constrained to yield approximately the long-term fault slip rates for the various segments [Table 3; *Working Group on California Earthquake Probabilities*, 2003]. Creep at seismogenic depth may compound the slip rate contributed by the earthquake cycle on partially creeping faults. An assignment of 4 mm/yr and 3 mm/yr to the "seismogenic" creep rate of the northern Hayward fault and Concord-Green Valley fault, respectively (Table 3), accounts for slow inferred deep creep of these segments [*Schmidt et al.*, 2005; *Working Group on California Earthquake Probabilities*, 2003] and helps complete the total budget of slip across the SFBR (Figure 3).

The recurrence interval for the peninsular SAF is based on ruptures having occurred at or near the Santa Cruz Mountains in 1838 and \sim 1640 (1600-1670) [*Schwartz et al.*, 2006]. Although there is no direct evidence for the 1838 rupture having extended further south than the Santa Cruz Mountains, or for the 1640 rupture having extended north thereof, the slip budget of the peninsular SAF can be rationalized by assuming a large degree of overlap between the 1838 and 1640 ruptures. In order to achieve a long term slip rate of the peninsular SAF of \sim 17 mm/yr [*Working Group on California Earthquake Probabilities*, 2003], repeated 1906-type ruptures are not sufficient because the recurrence interval for a very long SAF rupture is about 400 years, and 1906 slip along the peninsula was generally less than 4 meters. The addition of 1838-type earthquakes helps complete the expected slip budget of the peninsular SAF (e.g., Figure 3). Regardless of whether a preceding peninsular SAF rupture occurred simultaneously with the \sim 1640 event identified in the Santa Cruz Mountains, the supposition of such an earthquake occurring with roughly a 200 year recurrence interval is sufficient to complete the slip budget on the peninsula.

The recurrence interval T for the Hayward fault of 140 years (Table 2) is a compromise between estimates of $T = 151 \pm 23$ years (± 2 standard deviations) for the period AD 350-1868 [*Lienkaemper and Williams, 2006*] (revised to $T = 170 \pm 82$ years by *Lienkaemper and Williams, 2007*) and $T = 130 \pm 40$ years for the period AD 1470-1868 [*Lienkaemper et al., 2002*]. In light of the shorter T for the past 500 years, we believe that 140 years mean recurrence time is a conservative estimate for purposes of forecasting future behavior of the fault. Over both quoted time spans, the associated uncertainties are considerably smaller than those considered by *Working Group on California Earthquake Probabilities [2003]*.

Each listed earthquake (that occurs at time t_i with repeat time T_i) generates a countably infinite set of preceding earthquakes that occur at times $\{t_i - nT_i \mid n = 1, 2, \dots\}$. The times of the listed ruptures and their associated preceding events since 1650 are shown in Figure 4. Viscoelastic relaxation from past earthquakes that contribute substantial signals to the recent stress evolution is dominated by the contributions of the most recent events in a quasi-repeating sequence [e.g., *Meade and Hager, 2004*]. Therefore, the listed repeat times in Table 2 generally correspond to paleoseismic estimates based on the most recent history of faulting along each rupture. An exception is the assignment of $T = 124$ years to the 1989 earthquake, based on the hypothesis that a similar-sized earthquake that occurred in 1865 had ruptured the same area [*Bakun, 1999*], though likely somewhat to the northeast of the Loma Prieta rupture zone [*Yu and Segall, 1996*].

Kinematic self-consistency may be checked against the long-term slip rates integrated across the plate boundary zone. Figure 3 shows the fault-parallel long-term velocity on three profiles crossing the plate boundary zone. All three profiles are consistent with a net

~ 38 mm/yr right-lateral motion, in good agreement with geodetic estimates [e.g., *Argus and Gordon*, 2001]. In profile 1, this is achieved by the inclusion of the southern Calaveras fault as a creeping fault (dashed fault in Figure 2) with a slip rate of 16 mm/yr. As shown in the discussion leading to eqn (21), the time-dependent stress field is formally insensitive to the slip rate assigned to a steadily-creeping fault which is associated with no episodic slip events. However, this slip rate is constrained by the requirement to complement the neighboring long-term slip rates and match the overall tectonic relative motion. This is achieved with a slip rate on the southern Calaveras fault which approximately equals the summed long-term slip rates on Hayward and northern Calaveras faults (Table 3). If we were to evaluate the net long-term slip rates on profiles north of profile 3, then some source of long-term slip along the northern extension of the Rodgers Creek fault would need to be specified. As one endmember, this could be achieved with a creeping fault associated with steady slip at the same rate as the long-term slip rate of the Rodgers Creek fault (10 mm/yr). The other endmember possibility is a distribution of locked fault(s) with an uncertain history but with long-term slip rate of 10 mm/yr. Either possibility would provide the needed source of long-term slip in this region and, as shown in section 4, either possibility is consistent with the stressing history calculated with eqn (21). Similar reasoning may be used to provide sources of long-term slip south of the study area near 37°N where the model faults terminate.

Note that the set Ω_{unknown} described in section 4 contains, at least in part, faults with unknown slip history. These faults would be equivalent to the "background faults" used by *Working Group on California Earthquake Probabilities* [2003]. Although such faults themselves have a high collective probability of rupture in the SFBR [*Working Group on*

California Earthquake Probabilities, 2003], they cannot be readily included in the present framework. Rather, they serve the purpose of extending the included faults beyond the limited model region and supplying additional (unspecified) structures to allow kinematic self-consistency to be attained.

For a few faults, compromises have been made between disparate pieces of information. The southern Hayward fault ruptured with approximately 1.9 m right-lateral slip in 1868 [Yu and Segall, 1996]; we choose a slightly lower value of 1.8 m slip. Combined with a recurrence interval of 140 years, this results in a long-term slip rate of 12.8 mm/yr. This is considerably larger than the 8.8 mm/yr given by *Working Group on California Earthquake Probabilities* [2003], but the larger value is reasonable given that the maximum recorded creep rate of 9.2 ± 1.3 mm/yr [Lienkaemper and Borchardt, 1996] is considered a minimum bound for the long-term slip rate at seismogenic depth [Lienkaemper et al., 1991; Lienkaemper and Borchardt, 1996]. If the 1868 slip is indeed representative of the typical repeating southern Hayward fault slip event, then it implies that all long-term slip is released seismically below the creeping section (which we have assumed for simplicity to occupy the upper 5 km of the southern and northern Hayward faults). This is consistent with an "R-value" of 0.6 used by *Working Group on California Earthquake Probabilities* [2003], which can be interpreted in terms of a fault that creeps at the full (long-term) slip rate in its upper portion and is completely locked beneath that depth. The long-term slip rate used by *Working Group on California Earthquake Probabilities* [2003] is based chiefly on geodetic observations of strain accumulation at the surface, but such observations are very difficult to uniquely interpret [e.g., Savage et al., 1999] because of the presence of multiple fault strands and uncertainty in the mechanism of strain accumulation. Indeed,

Savage et al. [1999] obtain a geodetic slip rate of 16.6 ± 5.9 mm/yr on the Hayward fault. We suggest that a slip rate of 12.8 mm/yr and $R= 0.67$, consistent with fully creeping fault in the upper 5 km and a fully locked fault in the nominal seismogenic depth interval 5 to 15 km, is plausible for the southern Hayward fault.

The Concord-Green Valley (GV) fault is assigned a long-term slip rate of 7.5 mm/yr (Figure 3), of which 4.5 mm/yr is released seismically in 1700-type events (Table 2) and 3 mm/yr is assumed to be released through creep. This completes the budget of slip across Profile 3 to 39.0 mm/yr, the SAF and Rodgers Creek fault contributing 21.5 mm/yr and 10.0 mm/yr, respectively. Our long-term slip rate of 7.5 mm/yr is slightly larger than a documented slip rate of ~ 5 mm/yr [*Working Group on California Earthquake Probabilities*, 2003]. The needed slip rate on the Concord-GV fault could be reduced if ~ 2 mm/yr slip on the adjacent Greenville fault were included [*Working Group on California Earthquake Probabilities*, 2003], or if the northern SAF accommodated a greater amount of long-term slip. On the other hand, a slip budget totaling more than 38 mm/yr would encourage relatively high slip rates on the Concord-GV fault (as well as other faults). Using a viscoelastic coupling model *Savage et al.* [1999] obtain a long-term slip rate of 8.1 ± 2.0 mm/yr on the Concord-GV fault and a total slip rate of 41 mm/yr across the entire fault system. With the assigned 4.5 mm/yr seismic slip rate and a fault length of 60 km, which would have all slip taking place in repeated Concord + northern Green Valley + southern Green Valley slip events, the moment magnitude of the repeating slip events would be 7.10 (Table 2).

5.2. Regional stress evolution

Sets of postseismic relaxation after infinite sequences of characteristic earthquakes over the region are calculated using the viscoelastic normal mode method of *Pollitz* [1997] on the rheology model for the SFBR derived by *Pollitz and Nyst* [2004] (Figure 5, taking mantle viscosity $\eta_m = 1.2 \times 10^{19}$ Pa s). These are appended to the coseismic deformation field calculated for each earthquake [*Pollitz*, 1996]. Time-dependent stress at 8 km depth is calculated on a regular grid using equations (21) and (22). All stresses are referred to the state of stress that existed just before an arbitrary starting time of 1656, a time that is 250 years before the 1906 event on the SAF. Thus all points are assigned zero initial stress state at $t_0 = 1656$ just before the event. Supplementary Figures S1 to S4 and animation file S5 show 39 snapshots of Coulomb failure stress [*King et al.*, 1994] assuming a receiver fault geometry with strike 326° , dip 90° , and rake 180° (i.e., the geometry to produce a right-lateral rupture on the southern Hayward fault) with an effective friction coefficient of 0.4. Time-dependent stress patterns show the effects of stress shadows generated instantaneously at the times of the model earthquakes, subsequent viscoelastic relaxation, and gradual reloading of the plate-boundary system. The average stress accumulation rate of ~ 0.1 bars/yr is consistent with the geodetically-measured deformation rates in the SFBR [e.g. *Savage et al.*, 1998; *Pollitz and Nyst*, 2004].

The stress evolution fulfills expectations in the sense that all segments are relatively highly stressed just prior to the occurrence of a rupture on that segment. Nevertheless, the stress evolution along a particular segment is sensitive to the order of faulting. For example, the northern Hayward fault which ruptured in 1705 is predicted to lie in the stress shadow of the 1700 Concord-Green Valley event, and the Rodgers Creek fault

which ruptured in 1740 is predicted to lie in the stress shadow of the 1720 northern SAF event. Thus these faults were more highly-stressed just prior to the 1700 and 1720 events, respectively, than they were when they supposedly occurred. Stress triggering of the northern-Hayward and Rodgers-Creek events would be more plausible had they occurred somewhat earlier than the Concord-Green Valley and northern SAF events, respectively. Such revisions to the earthquake chronology are well within the uncertainties of the estimated rupture times of all segments concerned (Table 2).

5.3. Stress history of faults

Figure 6 shows the evolution of Coulomb failure stress at ten target points (locations indicated by black triangles in Figure 2) at 8 km depth as a function of time at the ten target points. The curves exhibit coseismic offsets, postseismic stressing (vigorous where the curves are strongly concave-upward or downward), and background interseismic loading. The viscoelastic relaxation component produces different effects on the stress field depending on distance from the source fault. This is seen by the stress evolution in the decades after 1906 but before 1989. Near the source fault its effect is to rapidly reload the surrounding crust, but more than about one elastic-plate thickness away (horizontally) its effect is to enhance the shadow. Note the concave-upward curvature of the stress curves of the Hayward fault and SAF, and the concave-downward curvature of the stress curves of the Concord-Green Valley fault, after 1906. Between 1910 and 1920 the shadow around the San Andreas fault is rapidly eroded by viscoelastic relaxation (net postseismic stressing rates exceed the background loading rate) while the shadow around the Concord-Green Valley fault (and other points to the east of the SAF) is eroded much less rapidly because the net postseismic stressing rate is less than the background stressing rate. This

effect and its time-transgressive behavior (the gradual enlargement of the stress reloading area around the source fault) is documented in similar studies [e.g., *Kenner and Segall, 1999; Pollitz et al., 2004*].

Assuming that each fault is associated with a definite Coulomb stress value at which the fault will fail, these stress curves are a guide to assessing how closely stress on a given fault has come to returning the fault to failure. With the set of assumed parameters used in these calculations (Tables 1 and 2), parts of many regional faults have (as of 2006) reached stress values close to those attained just prior to the last rupture. Examining points #1 and 2 on the southern Hayward fault, it is clear that the stress value in 2000 has returned to near its value that existed just before the last earthquake in 1868, and near its value that existed just before the preceding idealized earthquake in 1728. This supports the notion that the southern Hayward fault is approaching the end of its current cycle [e.g., *Lienkaemper et al., 2002*]. Along the peninsular SAF (points #3 and 4), stress values exceed those attained just prior to 1906 but are well below those attained just prior to 1838. From past history, the peninsular SAF can rupture either independently (1838-type) or with long (1906-type) ruptures. If the present model is a useful guide, then only an 1838-type rupture is presently possible because the N SAF (point #5) has a present stress value well below the pre-1906 stress value. Elsewhere, a return to stress levels attained before the preceding earthquake is predicted within ~ 25 years (Rodgers Creek, N Calaveras) to ~ 50 years (N Hayward, Concord-Green Valley).

6. Probabilities of future ruptures

6.1. Uncertainties in earthquake forecasting

The conditions necessary for earthquakes to re-rupture a given fault segment are generally complicated and depend on absolute stress distribution, fault geometry, material properties, and stressing history (including the date of most recent rupture for a pre-historic earthquake) [*Working Group on California Earthquake Probabilities*, 2003]. Since most of these factors are poorly known, they introduce epistemic uncertainty into any methodology that could be conceived to determine the initiation time of a future large rupture. In the context of the relatively simple model presented here, epistemic uncertainties include the sets of mean recurrence times $\{T_i\}$, slip distributions $\{u_i\}$, and time of last earthquake t_i (which is uncertain for pre-historic earthquakes), where index i refers to an event listed in Table 2. An additional epistemic uncertainty is the viscoelastic structure. An aleatory uncertainty is also introduced: the failure stress value associated with a future rupture, i.e., the stress level necessary to initiate rupture at a given point that results in a large rupture on that segment. We view this as reflecting randomness in physical conditions on the fault, and randomness in the situation that a representative point will initiate a rupture or fail as part of a rupture initiated elsewhere.

Using the forward-modeling framework of sections 3 and 4, we shall formally consider the impact of a four-fold set of uncertainties in model parameters on the inferred re-rupture times of individual segments. This proceeds from the randomization of four controlling parameters of the physical model with associated randomization in stressing history: 1. mean recurrence times $\{T_i\}$, 2. slip distributions $\{u_i\}$, 3. time of the last earthquake t_i (known for historic earthquakes; uncertain for pre-historic earthquakes), and 4. the

applicable failure stress level on the faults. Monte Carlo simulation is used to implement the random perturbations in these parameters.

If the failure stress level does not change, the predicted rupture time of a point \mathbf{r} , associated with fault segment i , is given by

$$t_R^{(i)}(\mathbf{r}) = t_{\text{Ref}} - \frac{\sigma(\mathbf{r}, t_{\text{Ref}}) - \sigma(\mathbf{r}, t_i^-)}{\dot{\sigma}(\mathbf{r}, t)|_{t=t_{\text{Ref}}}} \quad (\mathbf{r} \in \text{segment}\#i) \quad (24)$$

where t_{Ref} is a reference time which we take to be the present (i.e., 2006). Eqn (24) is the first-order Newton's-method estimate of the predicted rupture time, which is assumed to occur at the same stress level as existed just prior to the preceding earthquake on segment i , i.e., at time t_i^- . In the general case, the failure stress level associated with the next event may differ from that of the preceding event by an amount $\epsilon_1(\Delta\sigma)$, where ϵ_1 is a random variable and $\Delta\sigma$ represents a stress fluctuation. Then the predicted rupture time is given by

$$t_R^{(i)}(\mathbf{r}) = t_{\text{Ref}} - \frac{\sigma(\mathbf{r}, t_{\text{Ref}}) - \sigma(\mathbf{r}, t_i^-) + \epsilon_1(\Delta\sigma)}{\dot{\sigma}(\mathbf{r}, t)|_{t=t_{\text{Ref}}}} \quad (\mathbf{r} \in \text{segment}\#i) \quad (25)$$

It would be possible to make $\Delta\sigma$ dependent on location, but we assume here that it is a constant for all segments. Note that $t_R^{(i)}(\mathbf{r})$ in eqn (25) is explicitly dependent on the Coulomb failure stress threshold (which has a random component controlled by $\Delta\sigma$) and implicitly dependent on mean recurrence times $\{T_i\}$, slip distributions $\{u_i\}$, and earthquake occurrence times t_i^- through the dependences of the stress functions $\sigma(\mathbf{r}, t_{\text{Ref}})$, etc. Uncertainties in these other parameters will be quantified in the next sections.

With eqn (21), a set of realizations of stressing histories may be generated and, with eqn (24) or eqn (25), used to derive probability distributions of the time of re-rupture of the various fault segments.

6.2. Constraint on summed long-term slip rate

In simulations involving perturbations to slip u_i and mean recurrence time T_i on the fault segments, it is desirable to limit those perturbations to those combinations that preserve the ~ 38 mm/yr total relative motion across the plate boundary zone. To be more precise, segment $\#i$ generally has a characteristic seismic slip u_i , creep rate v_i^{creep} , and recurrence interval T_i . Note that v_i^{creep} is meant to be the creep rate which occurs over the same depth range as seismic slip for a given segment, so that it complements the long-term slip rate contributed by seismic slip. (Referring to Table 3, this is relevant for the northern Hayward and Concord-Green Valley faults, which have 3 mm/yr creep rate, and the southern Calaveras fault, which has a 16 mm/yr creep rate. As explained in section 4, fault creep plays no explicit role in loading the system. It is considered only to balance the budget of long-term slip.) In all simulations, we require that along each of the three profiles indicated in Figure 3, the summed long-term relative crustal velocity must lie within a plausible range of Pacific-Sierra Nevada relative plate motion, i.e., from 36 to 41 mm/yr:

$$\left| \sum_{i \in \text{profile}} \left[\frac{u_i}{T_i} + v_i^{\text{creep}} \right] - 38.5 \text{ mm/yr} \right| \leq 2.5 \text{ mm/yr} \quad (26)$$

6.3. Probabilities based on uncertainties in mean recurrence times

We first consider probability distributions of expected rupture times on the segments resulting from randomizing $\{T_i\}$. The mean recurrence times are represented in the form

$$T_i = (T_i)_0 + \epsilon_2(\Delta T_i) \quad (27)$$

where ϵ_2 is a random variable, ΔT_i is a timescale which may depend on the fault segment under consideration, and $(T_i)_0$ is the a-priori recurrence time prescribed in Table 2. The

cumulative stress given by eqn (21) depends upon continuous functions of T_i (second and third terms of eqn (21)) and discontinuous functions of T_i (first term of eqn (21)). For evaluation times t after the last earthquake in the collection, the first term remains constant. Eqn (22) combined with eqn (5) yields a dependence of the third term of eqn (21) – $[\dot{\sigma}_{load}(\mathbf{r})]_{\Omega_{known}} \times (t - t_0)$ – that varies with a $(T_i)^{-1}$ dependence from each contributing term in eqns (22) and (5). Thus the first and third terms of eqn (21) may be calculated with an initial set of $\{T_i\}$ (i.e., the $\{(T_i)_0\}$) and the third term rescaled with the revised T_i for each contributing segment.

The probability density functions associated with $\{T_i\}$ play a central role in determining the probabilities of future ruptures. It is generally difficult to estimate T_i for a given segment, and associated uncertainties in T_i are, with the exception of the south Hayward fault, poorly constrained. A useful constraint among the set $\{T_i\}$ is that summed slip rates should approximately equal the long-term slip rate across the plate boundary zone, and this constraint is exploited by *Working Group on California Earthquake Probabilities* [2003] and here (eqn (26)). As for the choice of probability density, the Gaussian distribution (for an estimate T with standard deviation σ_T) tends to be strongly peaked on the mean value, with 32% of possible realizations falling between one and two standard deviations of the mean. However, the uniform distribution over the interval $[T - 2\sigma_T, T + 2\sigma_T]$, covering two two standard deviations on either side of the mean, has 50% of possible realizations falling between one and two standard deviations of the mean. Although the Gaussian tail of $\sim 5\%$ of possible realizations is eliminated by this uniform distribution, it is of no practical consequence, and resulting rupture probabilities are invariably broadened by using the uniform distribution rather than the Gaussian distribution. For the

southern Hayward fault, *Lienkaemper et al.* [2002] obtain a mean recurrence interval of 130 years and standard deviation of 20 years for the period AD 1470-1868. We make two choices which slightly broaden the resulting future rupture probability: 1. We assign a mean recurrence interval of 140 years (section 5.1), and 2. We use eqn (26) with $\epsilon_2 = U[-1, 1]$ (the uniform distribution over the interval $(-1, 1)$) and $\Delta T = 42$ years, i.e., a uniform distribution covering slightly greater than two standard deviations about the mean. Apart from eqn (26), there are little quantitative constraints on uncertainties in recurrence interval for other faults, and we assign generally $\Delta T_i = 0.3 \times T_i$ when employing eqn (27).

Using the above choices of ϵ_2 and ΔT_i , estimates of rupture time at ten points on area faults (Figure 2) are generated by substituting eqn (27) into eqn (24) and using eqn (24) with 1000 realizations of $\{T_i\}$. Only those realizations that result in rupture times in the future (≥ 2006) are retained, so that the resulting probability distributions are conditional probability distributions given that the re-ruptures have not yet occurred. The solid curves of Figure 7 show the cumulative probability distributions of rupture time at these points. The probability distributions are generally spread out over a period of several decades, but the southern Hayward fault is exceptional in the narrowness of the cumulative probability distribution, all of the randomized rupture times occurring before 2040 with a formal probability of 100%.

6.4. Probabilities based on combined uncertainties

We next randomize the slip distributions of the repeating ruptures $\{u_i\}$ simultaneously with the mean recurrence times $\{T_i\}$. We choose to represent slip of segment #i as

$$u_i = (u_i)_0 \times (1 + b \epsilon_3) \tag{28}$$

where ϵ_3 is a random variable, b is a constant, and $(u_i)_0$ is the a-priori slip distribution of the segment. (It may be variable along a segment, and eqn (28) means that the slip values of all subsegments belonging to segment $\#i$ are scaled by the identical amount $b\epsilon_3$.) We assign $\epsilon_3 = U[-1, 1]$ and take $b = 0.2$, i.e., up to 20% random variations in assigned slip distributions with a $\pm 10\%$ average. The dashed curves of Figure 7 show the cumulative probability distributions resulting from randomizing both $\{T_i\}$ and $\{u_i\}$. Comparing the two sets of curves in Figure 7, there is remarkably little change resulting from randomizing the slip distributions. This is because changing the slip distribution on a segment produces a corresponding change in the loading rate along the same segment, via eqns (5) and (22), which acts in the opposite direction. Slight changes in the stress buildup along a segment are propagated through the newly randomized stress changes imparted by neighboring segments. However, this results in only a slight broadening of the probability distributions which is barely discernable in Figure 7.

With the uncertainties $\{T_i\}$ and $\{u_i\}$ we combine uncertainties in Coulomb failure stress threshold and uncertainties in the last rupture times t_i of pre-historic earthquakes. The former is realized by randomizing the stress threshold with eqn (25), assigning $\epsilon_1 = U[-1, 1]$, and taking $\Delta\sigma = 4$ bars. The latter is randomized via

$$t_i^- = (t_i)_0 - 0 + c_i \times \epsilon_4 \quad (29)$$

where $\epsilon_4 = U[-1, 1]$, c_i is a segment-specific constant, and $(t_i)_0$ is the last rupture time of the segment. We assign $c_i = 0$ to a segment associated with a historic rupture and $c_i = 50$ years to a segment associated with a pre-historic rupture. Eqn (25) would suggest that, if the loading rate at the time of a pre-historic earthquake were similar to that at time t_{Ref} and associated perturbations in viscoelastic relaxation were neglected, then a

shift in t_i^- would be matched by an identical shift in $t_R^{(i)}(\mathbf{r})$ for any point \mathbf{r} on the rupture of event $\#i$. This is true as long as the shift in t_i does not cross a discontinuity in $t_R^{(i)}(\mathbf{r})$ as a function of t_i^- , which can occur if the perturbed rupture time is near the rupture time of another segment. For example, a perturbation in the time of the ~ 1705 northern Hayward fault event which resulted in an assigned last rupture date of 1695 would have this event occur before the ~ 1700 Concord-Green Valley fault event. In the perturbed case, the stress state at $t_i^- = 1695$ has not been affected by the occurrence of the 1700 earthquake. In the unperturbed case, the 1705 rupture zone lies in the shadow of the 1700 earthquake. The expected time for re-rupture of the northern Hayward fault would be retarded because of the perturbation in t_i^- , despite the fact that the perturbation would advance the re-rupture time by 10 years if the Concord-Green Valley fault played no role. This effect is embodied in the definition of $\sigma(\mathbf{r}, t_i^-)$, which appears in eqn (25), and it is taken into account in the Monte Carlo simulations.

The solid curves of Figure 8 show the probability distributions using all combined uncertainties and the same viscoelastic structure as previously, i.e., the *Pollitz and Nyst* [2004] viscoelastic structure with mantle viscosity $\eta_m = 1.2 \times 10^{19}$ Pa s. The dashed curves in Figure 8 show the result using all combined uncertainties under the limit $\eta_m \rightarrow \infty$. (The same limit applies to crust viscosity in this viscoelastic model.) This is the case of a block model of crustal strain accumulation and release, where interseismic strain accumulation proceeds at constant rates owing to the arbitrarily large viscosity of the substrate below the elastic layer [*Savage*, 1983; *Savage et al.*, 1999]. The effect of raising the viscosity of the ductile substrate is, relative to the low-viscosity case, to deepen the 1906 stress shadow along the SAF itself (viscoelastic reloading and erosion of the stress

shadow proceeds at a slower rate) and to reduce the stress shadow on surrounding faults (viscoelastic enhancement of the stress shadow proceeds at a slower rate). The net effect is to shift the probability distributions to later times for the various SAF segments and shift the probability distributions to earlier times (i.e., advance the expected future rupture time) for the surrounding faults.

7. Discussion

The faults exhibiting consistently the highest future hazard, regardless of randomization strategy, are the southern Hayward, Rodgers Creek, and northern Calaveras faults. Different randomization strategies produce different shapes and durations of the probability distributions. The strongest factors affecting the probability distributions are the uncertainties in mean recurrence times, uncertainties in failure stress threshold, and uncertainties in the time of last rupture, i.e., ΔT_i , $\Delta\sigma$, and t_i . (The last is uncertain only for pre-historic ruptures.) Perturbations in characteristic slip u_i have a relatively minor impact. The first three factors tend to broaden the probability distributions. For a fault that is nearly theoretically due to rupture, the mean expectation time of the next event on a given segment consequently tends to be retarded when these factors are included. As an endmember example, the expectation time of the next rupture of points #1 and 2 (i.e., southern Hayward fault) would be 2003 in the absence of perturbations in ΔT_i , $\Delta\sigma$, t_i , or Δu_i . The greater the magnitude of these random factors, the greater number of realizations yield occurrence times beyond 2006, and hence conditional probability distributions that become increasingly shifted to later times. On the other hand, for segments that are predicted to rupture only several decades from now (i.e., the northern SAF), the ef-

fect of these perturbations is to broaden the probability distributions without appreciably altering the mean expected occurrence time.

Using the present methodology to assess the seismic hazards of the peninsular SAF (which spans the zone of the idealized 1838 earthquake in Figure 2) is problematic. The rupture extent of the 1838 earthquake itself is uncertain, so that stress buildup at points #3 and 4 may be substantially different from that shown in Figure 6. For point #4, the present stress level is presently close to the stress level predicted just before the 1906 earthquake, but it is well below the stress level predicted just before the 1838 earthquake. The probability distribution for this point in Figures 7 and 8, which was derived assuming a return to pre-1838 stress levels, would be shifted substantially to the left (earlier predicted future rupture) if the pre-1906 stress level were the expected failure stress level (Figure 9). Although a repeat of the 470-km long 1906 rupture is unlikely in the coming decades because of the relatively low stress level along the northern SAF, a peninsular SAF rupture similar to the 1838 earthquake is possible. The 1906 earthquake itself was a bilateral rupture beginning at roughly 37.8°N [Wald *et al.*, 1993]. A unilateral rupture beginning at the same location and propagating southward, or beginning near the southern termination of the 1838 rupture and propagating northward, is conceivable. These possibilities would raise the seismic hazards of the peninsular segment to a greater level than suggested by Figures 7 and 8. If the pre-1906 stress state were indeed applicable, then at least the northern part of the peninsular SAF would have a future seismic hazard similar to that of the northern Calaveras fault (Figures 8 and 9).

Single-segment probabilities derived in the present study are generally different than those derived by *Working Group on California Earthquake Probabilities* [2003]. Figure

10 shows a comparison between the 30-year probabilities of $M \geq 6.7$ ruptures given by *Working Group on California Earthquake Probabilities* [2003] and the 30-year probabilities predicted by the stress evolution model for the finite and infinite-viscosity cases. The magnitude in the stress evolution model is unspecified, but we believe that it is comparable with $M \geq 6.7$ probabilities at least for those segments with demonstrated repeated ruptures at or exceeding that magnitude (e.g., HS, SAP). Stress-evolution probabilities are significantly higher than the weighted probabilities of *Working Group on California Earthquake Probabilities* [2003] for HS, HN, RC, and CN (Figure 10a) ; they are significantly lower for SAN, GVY, and SG. The much larger probabilities for HS, HN, and CN persist when compared with the BPT-renewal or BPT-step models (Figures 10b,c). There are many factors which contribute to these differences: 1. We approach future earthquake rupture times using a physical model to project stress into the future. 2. We exploit a recently-determined earthquake chronology, which strongly constrains the state of stress on many of the faults. 3. We adopt a likely oversimplified approach of forcing future ruptures to be exact replicates of large (and idealized) previous earthquakes on the various segments. Regarding factors 1 and 2, probability differences generally result from a systematic accounting of interseismic stress and stress interactions from surrounding faults. This implicitly includes the 1906 stress shadow as well as enhanced-stress/shadow zones from other faults. However, factor 3, if it were to be implemented, might reduce large-magnitude rupture probabilities on the Hayward, Rodgers Creek, and northern Calaveras faults. In the present approach, moment release on a given segment is not spread over a wide spectrum of magnitudes as it is in *Working Group on California Earthquake Probabilities* [2003]. Since a 39 mm/yr long-term velocity across the plate boundary is enforced,

the present model – if extrapolated several earthquake cycles into the future – must satisfy the long-term moment release rate. The question is whether past fault behavior, which is restricted here to large earthquakes, is a robust guide to future fault behavior. Variable segment behavior is implicitly included in the division of the 470 km-long 1906 rupture zone into shorter segments which may rupture in 1720-type or 1838-type earthquakes, which are smaller than 1906-type earthquakes. This could be carried further with finer segmentation of other Bay area faults. This would allow for future moment release to be accommodated by a greater number of small-magnitude events, which would remove part of the hazard assigned by the present model to future large ruptures. The present model is best interpreted as indicating when a given segment will return to the same state of stress that it had at the time of its last large rupture. A useful analogy is the Parkfield segment of the San Andreas fault, which had ruptured with nearly identical $M \sim 6.3$ earthquakes in 1922, 1934, and 1966, but only $M \sim 6.0$ in 2004 [Murray and Langbein, 2006]. The "gap" with previous ruptures was partially made up by a large amount of afterslip which exceeded the 2004 mainshock in seismic moment [Murray and Langbein, 2006]. The southern Hayward fault, as well as other Bay area faults, could conceivably change mode to a 2004-Parkfield type rupture. The timing of such a future Hayward-fault rupture may be well assessed by the present model, but the magnitude may not.

8. Conclusions

A kinematically self-consistent viscoelastic cycle model has been applied to the SFBR. The model is grounded in knowledge of historical earthquakes as well as estimates of the time and size of pre-historic earthquakes. Key inputs are the fault geometries of past ruptures (which are assumed to be periodic), their mean recurrence times, and the

viscoelastic structure. This information is used in the new framework to generate stress evolution in the regional crust since 1656 (arbitrarily chosen to be 250 years before the 1906 earthquake). Estimated time to future rupture(s) is calculated from the stress evolution and the value of Coulomb failure stress (at selected fault locations) just prior to the preceding earthquake on a given segment. Conditional probabilities of future ruptures are derived through Monte Carlo simulation by allowing epistemic uncertainty in the time of the last earthquake (for pre-historic ruptures), mean recurrence times, and slip magnitudes, and aleatoric uncertainty in the Coulomb stress thresholds.

Based on the criterion of a Coulomb failure stress threshold, the greatest seismic hazards are posed by the southern Hayward fault, Rodgers Creek fault, and northern Calaveras fault, in that order. This conclusion is also reached qualitatively by *Working Group on California Earthquake Probabilities* [2003]. The probability of rupture of the southern Hayward fault over the next 30 years is 40% to 75% when only uncertainties in mean recurrence times and slip magnitudes are factored in, and the same range even when uncertainties in Coulomb failure stress threshold are added. (There is a difference in that, in the latter case, the tail of the probability distributions at higher probability levels is longer.) These probabilities are much higher than those estimated for the southern Hayward fault by *Working Group on California Earthquake Probabilities* [2003]. They are similar to independent 30-year estimates of 64% or 39% given by *Lindh* [2005] without elaboration. The peninsular San Andreas fault is problematic to analyze in the present framework because it ruptured in both 1838 and 1906. Estimated time of next rupture depends on whether it is based on a return to pre-1838 or pre-1906 values. Since pre-1906 stress values were about 5 bars smaller, a rupture time based on a return to pre-1906

stresses would be achieved earlier than that based on a return to pre-1838 values. Using the pre-1906 stresses, this segment would have a 3% to 30% chance of rupturing during the next 30 years depending on where the hypothetical rupture were to nucleate. The higher value is near the 30-year estimates of 27% and 32% given by *Lindh* [2005].

Our focus on long-term stress evolution is meant to capture a possibly-predictable element of earthquake occurrence, i.e., fault behavior on a time scale of decades [*Sykes et al*, 1999]. Although the present study suggests higher rupture probabilities on several faults than given by *Working Group on California Earthquake Probabilities* [2003], several caveats must be considered when interpreting these probabilities. Our probabilities are conditional probabilities for future ruptures with a single-rupture scenario for the future; coupling and secondary stress interaction among two or more future ruptures are not considered. The assumptions of characteristic earthquakes with uniform recurrence intervals, as well as a laterally homogeneous Maxwellian viscoelastic structure, are overly simplistic. Most faults exhibit substantial aperiodicity [*Ellsworth et al.*, 1999], and paleoseismic data from other fault systems indicate fluctuations in fault slip rates on temporal scales of 100s to 1000s of years [*Jacoby Jr. et al.*, 1988; *Fumal et al*, 2002; *Bennett et al.*, 2004; *Weldon et al.*, 2004]. The rheology applicable to the Earth's lower crust and mantle is uncertain, and the viscoelastic structure is likely laterally variable given substantial lateral variability in seismic structure [*Humphreys and Dueker*, 1994] and heat flow [*Lachenbruch and Sass*, 1980; *Sass et al.*, 1989]. No attempt has been made to assess model uncertainty. This would require additional considerations, e.g., multiple representative points on a target fault, a range of plausible viscoelastic structures, and ruptures on other faults, including presently unrecognized faults (especially thrust faults accommodating fault-perpendicular

shortening). The model is designed to assess the time at which a given fault will return to the same state of stress as existed at the time of its last large-magnitude rupture. Given the many model simplifications and lack of model uncertainty, the rupture probabilities presented here are only a rough guide to future fault behavior and do not necessarily forecast the magnitude of a future event.

Acknowledgments. We thank Bill Bakun and Jim Savage for internal reviews, Tom Hanks for discussions, and Roland Bürgmann and Jeanne Hardebeck for comments on a preliminary draft. This paper benefitted from the constructive criticisms of Steve Cohen and two anonymous reviewers.

References

- Argus, D.F., and R.G. Gordon, Present tectonic motion across the Coast Ranges and San Andreas fault system in central California, *Geol. Soc. Am. Bull.*, 113, 1580-1592, 2001.
- Bakun, W.H., Seismic activity of the San Francisco Bay region, *Bull. Seismol. Soc. Am.*, 89, 764-784, 1999.
- Bennett, R., A. Friedrich, and K. Furlong, Slow-down and recovery of the San Andreas fault associated with San Jacinto fault inception from the inversion of geologic fault slip data, *Geology*, 32, 961-964, 2004.
- Ellsworth, W. L., M. V. Matthews, R. M. Nadeau, S. P. Nishenko, P. A. Reasenber, and R. W. Simpson, A physically-based earthquake recurrence model for estimation of long-term earthquake probabilities, *U.S. Geological Survey Open-File Report*, 99-522, 2003.

- Fumal, T.E., R.J. Weldon, G.P. Biasi, T.E. Dawson, G.G. Seitz, W.T. Frost, and D.P. Schwartz, Evidence for large earthquakes on the San Andreas fault at the Wrightwood, California paleoseismic site: A.D. 500 to Present, *Bull. Seismol. Soc. Am.*, *92*, 2726-2760, 2002.
- Humphreys, E. D., and K. G. Dueker, Western US upper mantle structure, *J. Geophys. Res.*, *99*, 9615-9634, 1994.
- Hardebeck, J. L., Stress triggering and earthquake probability estimates, *J. Geophys. Res.*, *109*, B04310, doi:10.1029/2003JB002437, 2004.
- Jacoby Jr., G.C., P.R. Sheppard, and K.E. Sieh, Irregular recurrence of large earthquakes along the San Andreas fault: Evidence from trees, *Science*, *241*, 196-199, 1988.
- Kenner, S.J, and P. Segall, Time dependence of the stress shadowing effect and its relation to the structure of the lower crust, *Geology*, *27*, 119-122, 1999.
- King, G.C.P., R.S. Stein, and J. Lin, Static stress changes and the triggering of earthquakes, *Bull. Seismol. Soc. Am.*, *84*, 935-953, 1994.
- Lachenbruch, A. H., and J. H. Sass, Heat flow and energetics of the San Andreas fault zone, *J. Geophys. Res.*, *85*, 6185-6223, 1980.
- Lienkaemper, J.J., G. Borchardt, and M. Lisowski, Historic creep rate and potential for seismic slip along the Hayward fault, California, *J. Geophys. Res.*, *96*, 18,261-18,283, 1991.
- Lienkaemper, J.J., and G. Borchardt, Holocene slip rate of the Hayward fault at Union City, California, *J. Geophys. Res.*, *101*, 6099-6108, 1996.
- Lienkaemper, J.J., T.E. Dawson, S.F. Personius, G.G. Seitz, L.M. Reidy, and D.P. Schwartz, A record of large earthquakes on the southern Hayward fault for the past

500 years, *Bull. Seismol. Soc. Am.*, *92*, 2637-2658, 2002.

Lienkaemper, J.J., and P.L. Williams, A 1650-year record of large earthquakes on the southern Hayward fault, *Seismol. Res. Lett.*, *77*, 229, 2006.

Lienkaemper, J.J., and P.L. Williams, A record of large earthquakes on the southern Hayward fault for the past 1700 years, *Seismol. Res. Lett.*, *in press*.

Lindh, A.G., Success and failure at Parkfield, *Seismol. Res. Lett.*, *76*, 3-6, 2005.

Marshall, G. A., R. S. Stein and W. Thatcher, Fault geometry and slip from coseismic level changes: the 18 October 1989, Loma Prieta, California, earthquake, *Bull. Seismol. Soc. Am.*, *81*, 1660-1693, 1991.

Meade, B.J., and B.H. Hager,, Viscoelastic deformation for a clustered earthquake cycle, *Geophys. Res. Lett.*, *31*, 10.1029/2004GL019643, 2004.

Michael, A. J., Viscoelasticity, postseismic slip, fault interactions, and the recurrence of large earthquakes, *Bull. Seismol. Soc. Am.*, *95*, 1594-1603, 2005.

Murray, J., and J. Langbein, Slip on the San Andreas fault at Parkfield, California, over two earthquake cycles, and the implications for seismic hazard , *Bull. Seismol. Soc. Am.*, *96*, S283-S303, 2006.

Parsons, T., S. Toda, R. S. Stein, A. Barka and J. H. Dieterich, Heightened odds of large earthquakes near Istanbul: An interaction-based probability calculation, *Science*, *288*, 661-665, 2000.

Pollitz, F. F., Coseismic deformation from earthquake faulting on a layered spherical Earth, *Geophys. J. Int.*, *125*, 1-14, 1996.

Pollitz, F. F., Gravitational viscoelastic postseismic relaxation on a layered spherical earth, *J. Geophys. Res.*, *102*, 17,921-17,941, 1997.

Pollitz, F. F., Viscoelastic shear zone model of a strike-slip earthquake cycle, *J. Geophys. Res.*, *106*, 26,541–26,560, 2001.

Pollitz, F. F., The relationship between the instantaneous velocity field and the rate of moment release in the lithosphere, *Geophys. J. Int.*, *153*, 595–208, 2003.

Pollitz, F.F., W.H. Bakun, and M.C.J. Nyst, A physical model for strain accumulation in the San Francisco Bay Region, II: Stress evolution since 1838, *J. Geophys. Res.*, *109*, B11408, doi:10.1029/2004JB003003, 2004.

Pollitz, F. F., and M. C. J. Nyst, A physical model for strain accumulation in the San Francisco Bay Region, *Geophys. J. Int.*, *160*, 302–317, 2004.

Pollitz, F. F., and M. C. Vergnolle, Viscoelastic deformation cycle model of the western United States instantaneous velocity field, *J. Geophys. Res.*, *in press*, 2006.

Sass, J., D. Blackwell, D. Chapman, J. Costain, E. Decker, L. Lawver, and C. Swanberg, Heat flow from the crust of the United States, in *Physical Properties of Rocks and Minerals*, edited by Y. S. Touloukian, W. R. Judd, and R. F. Roy, II-2, pp. 503–548, Hemisphere Publ. Corp., New York, New York, 1989.

Savage, J. C., and W. H. Prescott, Asthenospheric readjustment and the earthquake cycle, *J. Geophys. Res.*, *83*, 3369–3376, 1978.

Savage, J. C., A dislocation model of strain accumulation and release , *J. Geophys. Res.*, *88*, 4984–4996, 1983.

Savage, J. C., R.W. Simpson, and R.H. Murray, Strain accumulation rates in the San Francisco Bay area , *J. Geophys. Res.*, *103*, 18,039-18,051, 1999.

Savage, J. C., J.L. Svarc, and W.H. Prescott, Geodetic estimates of fault slip rates in the San Francisco Bay area , *J. Geophys. Res.*, *104*, 4995-5002, 1999.

Schmidt, D.A., R. Bürgmann, R.M. Nadeau, and M. d'Alessio, Distribution of aseismic slip rate on the Hayward fault inferred from seismic and geodetic data, *J. Geophys. Res.*, *110*, doi:10.1029/2004JB003397, 2005.

Schwartz, D., W. Lettis, J. Lienkaemper, S. Hecker, K. Kelson, T. Fumal, J. Baldwin, G. Seitz, and T. Niemi, The earthquake cycle on a plate boundary fault system: San Francisco Bay area 1600-2006, *Seismol. Res. Lett.*, *77*, 228, 2006.

Sykes, L. R., B. E. Shaw, and C. H. Scholz, Rethinking earthquake prediction, *Pure Appl. Geophys.*, *155*, 207-232, 1999.

Thatcher, W., G. Marshall, and M. Lisowski, Resolution of fault slip along the 470-km-long rupture of the great 1906 San Francisco earthquake and its implications, *J. Geophys. Res.*, *102*, 5353-5367, 1997.

Wald, D.J., H. Kanamori, D.V. Helmberger, and T.H. Heaton, Source study of the 1906 San Francisco earthquake, *Bull. Seismol. Soc. Am.*, *83*, 981-1019, 1993.

Weldon, R.J., K.M. Scharer, T.E. Fumal, and G.P. Biasi, Wrightwood and the earthquake cycle: what a long recurrence record tells us about how faults work, *GSA Today*, *14*, 4-10, 2004.

Working Group on California Earthquake Probabilities, Earthquake probabilities in the San Francisco Bay region, *U.S. Geological Survey Open-File Report*, *03-214*, 2003.

Yu, E., and P. Segall, Slip in the 1868 Hayward Earthquake from the analysis of historical triangulation data, *J. Geophys. Res.*, *101*, 16,101-16,118, 1996.

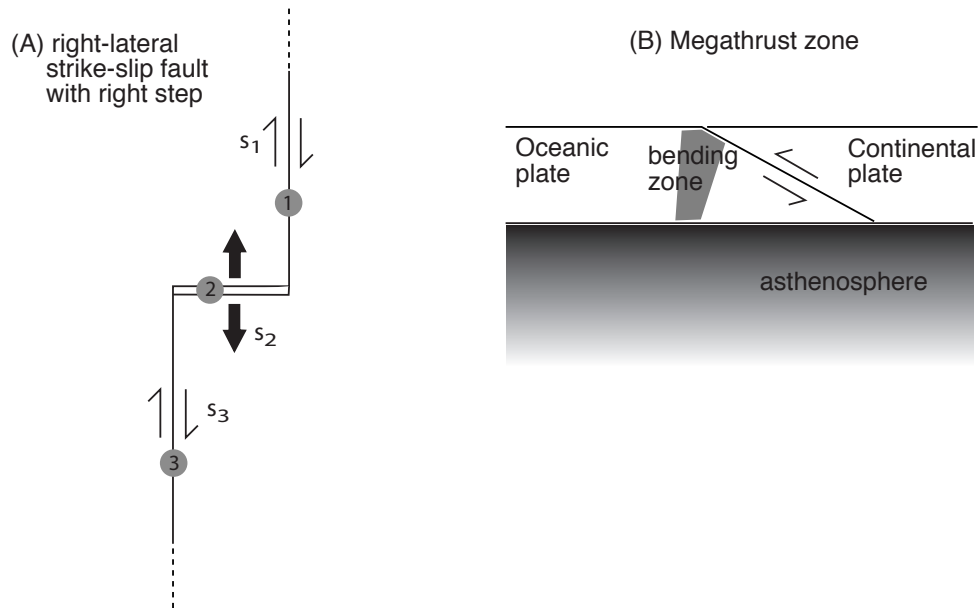


Figure 1. (a) Map view of a right-lateral strike-slip fault with a right step, where motion is accommodated by rifting. The associated slip rates are \dot{s}_1 and \dot{s}_3 for the strike-slip segments and \dot{s}_2 for the rifting segment. (b) Cross-section view of a megathrust zone. A thrust fault bounds oceanic and continental plates and penetrates to the base of the elastic layer.

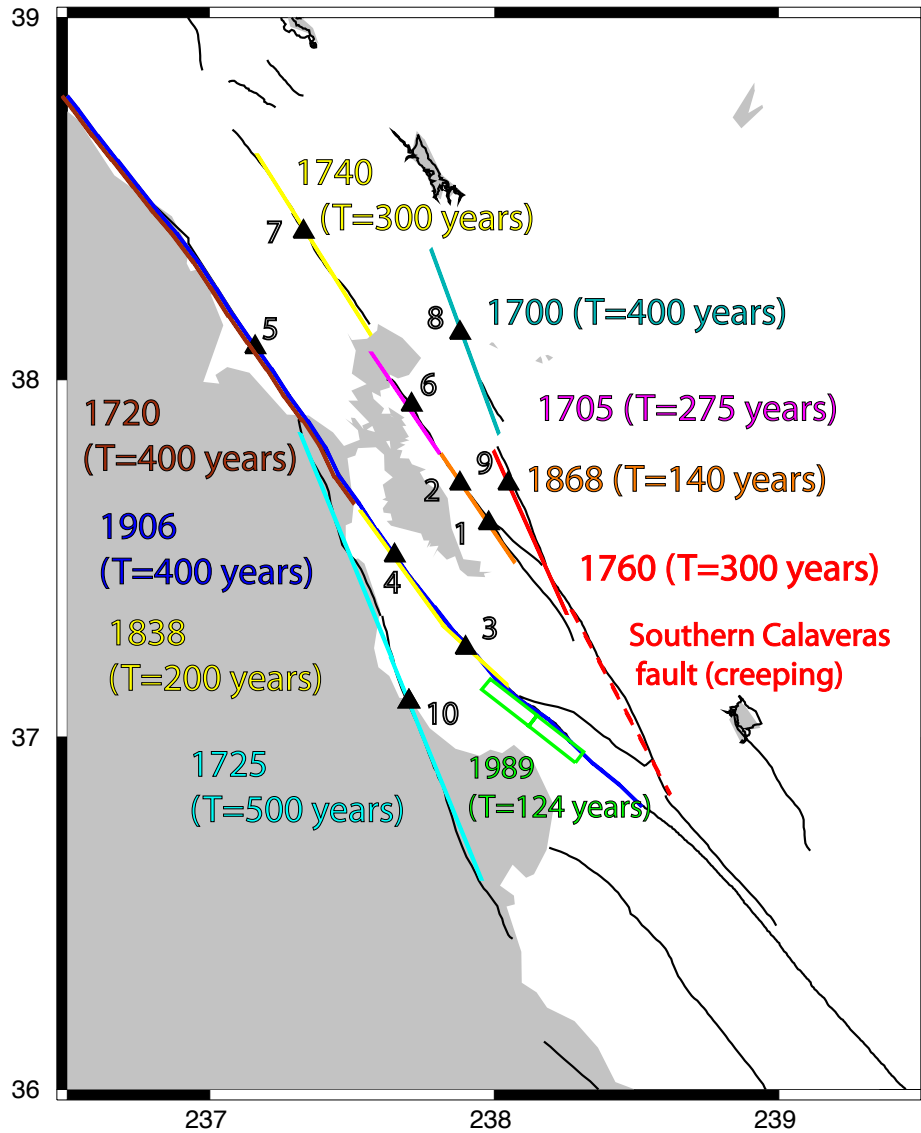


Figure 2. Rupture planes associated with the (estimated year) 1700, 1705, 1725, 1740, and 1760 pre-historic events and the (known year) 1868, 1906, and 1989 historic repeating sources. Triangles indicate the points where stress evolution is evaluated. Snapshots of this stress evolution are given in Supplementary Figures S1 to S4.

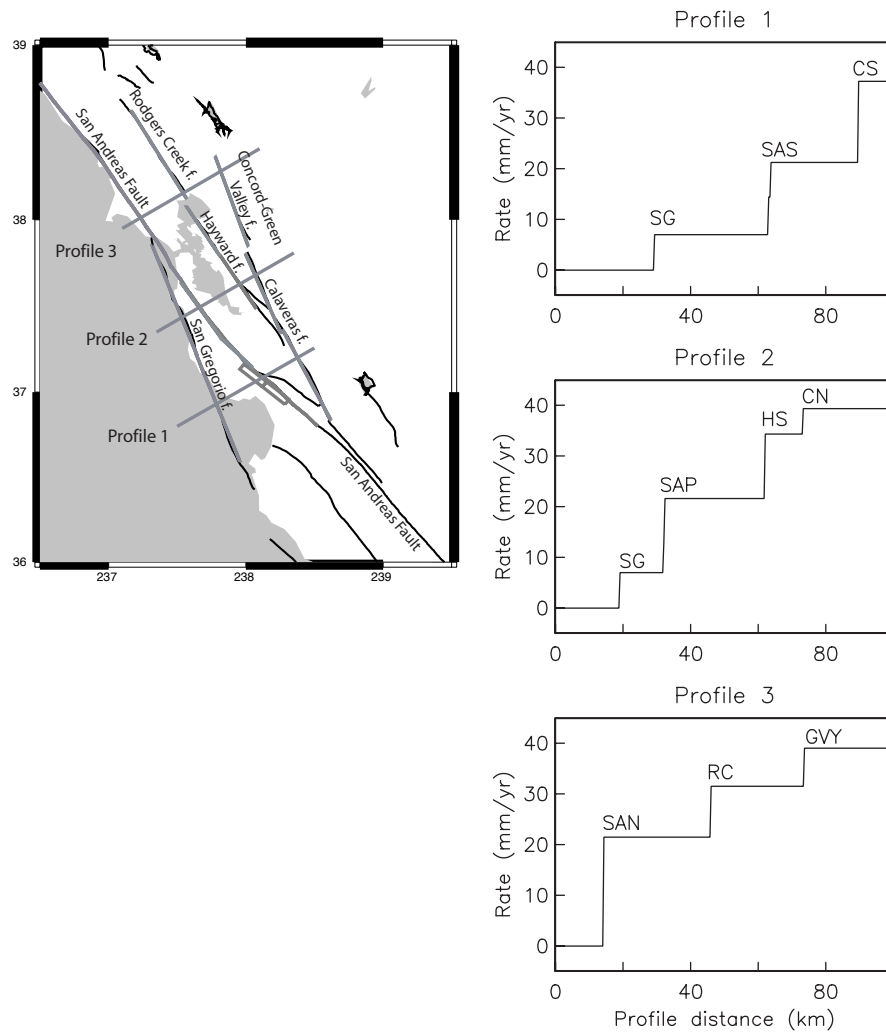


Figure 3. Long-term velocity of crust along indicated profiles. Jumps in velocity occur at fault crossings labeled as follows: GVY (Concord-Green Valley), SAN (San Andreas North), SAP (Peninsular San Andreas), SAS (Santa Cruz Mountains San Andreas), RC (Rodgers Creek), HS (South Hayward), CN (Northern Calaveras), CS (Southern Calaveras). The total 7.5 mm/yr jump across GVY includes 4.5 mm/yr slip released seismically and 3 mm/yr of creep (Table 3).

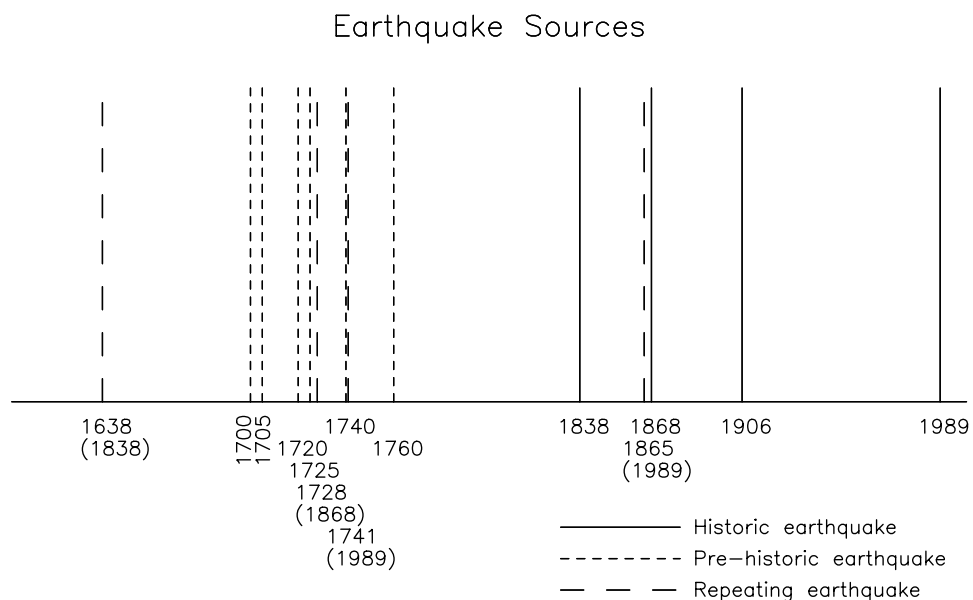


Figure 4. Rupture times of earthquakes listed in Table 2 plus their periodically-occurring preceding events. Preceding events are labeled with the time of the last earthquake in the sequence given in parentheses.

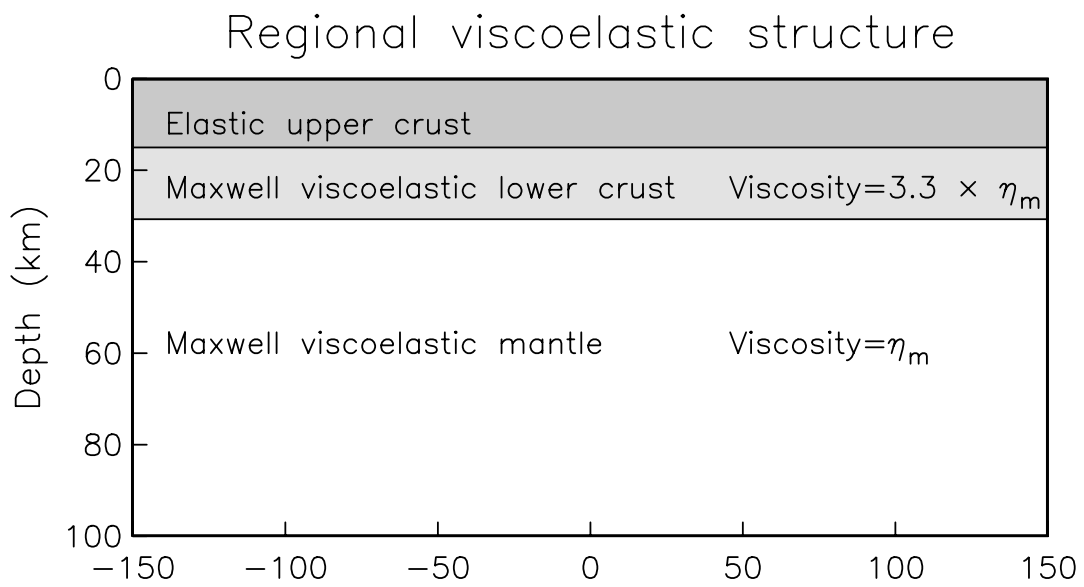


Figure 5. Viscoelastic stratification of the SFBR used in this study, consisting of an elastic upper crust underlain by Maxwell viscoelastic lower crust and mantle [*Pollitz and Nyst, 2004*].

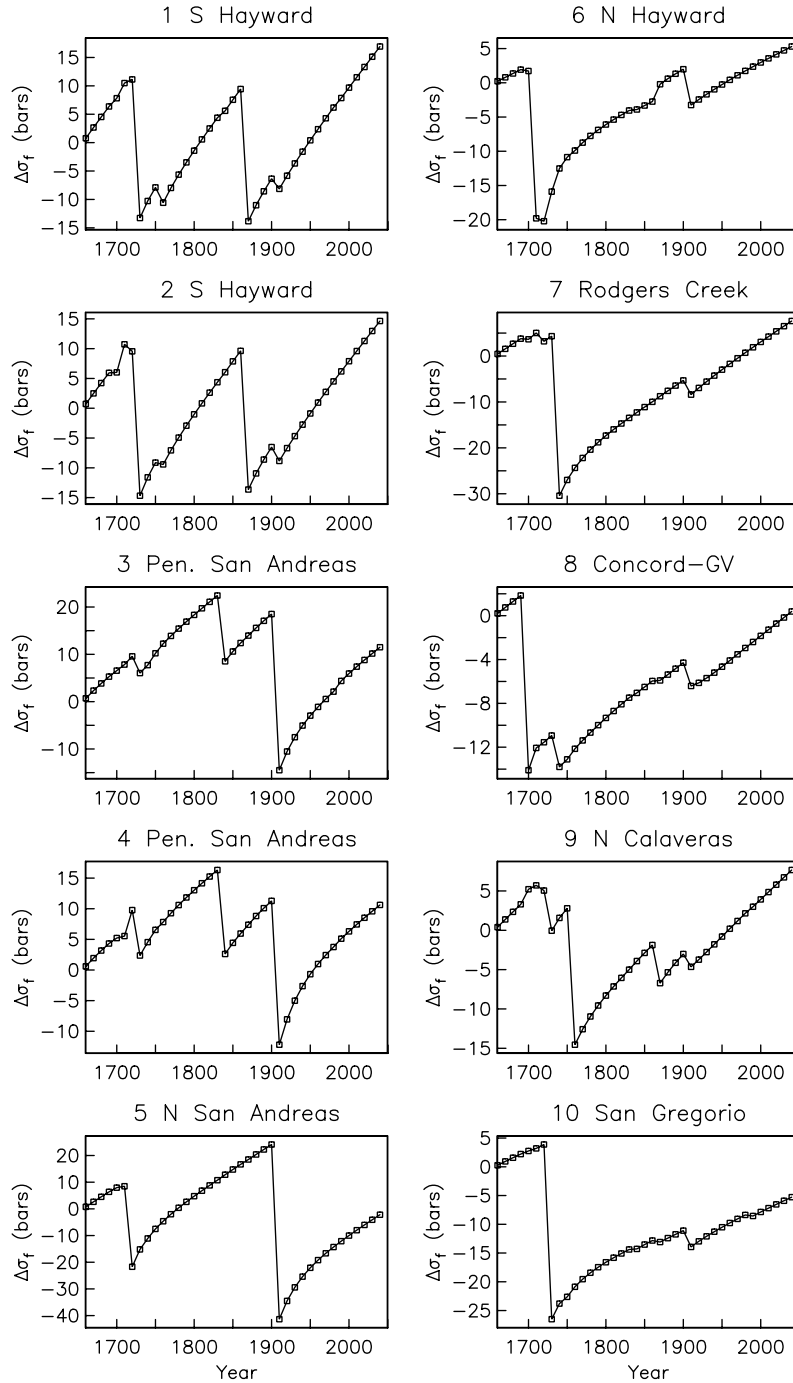


Figure 6. Time-dependent stress at ten points at 8 km depth (locations given in Figure 2) in increments of 10 years. $\Delta\sigma_f$ is the change in Coulomb failure stress accumulated since 1650. At these ten points the plotted $\Delta\sigma_f$ is identical to that plotted in Supplementary Figures S1 to S4 at 10 year intervals.

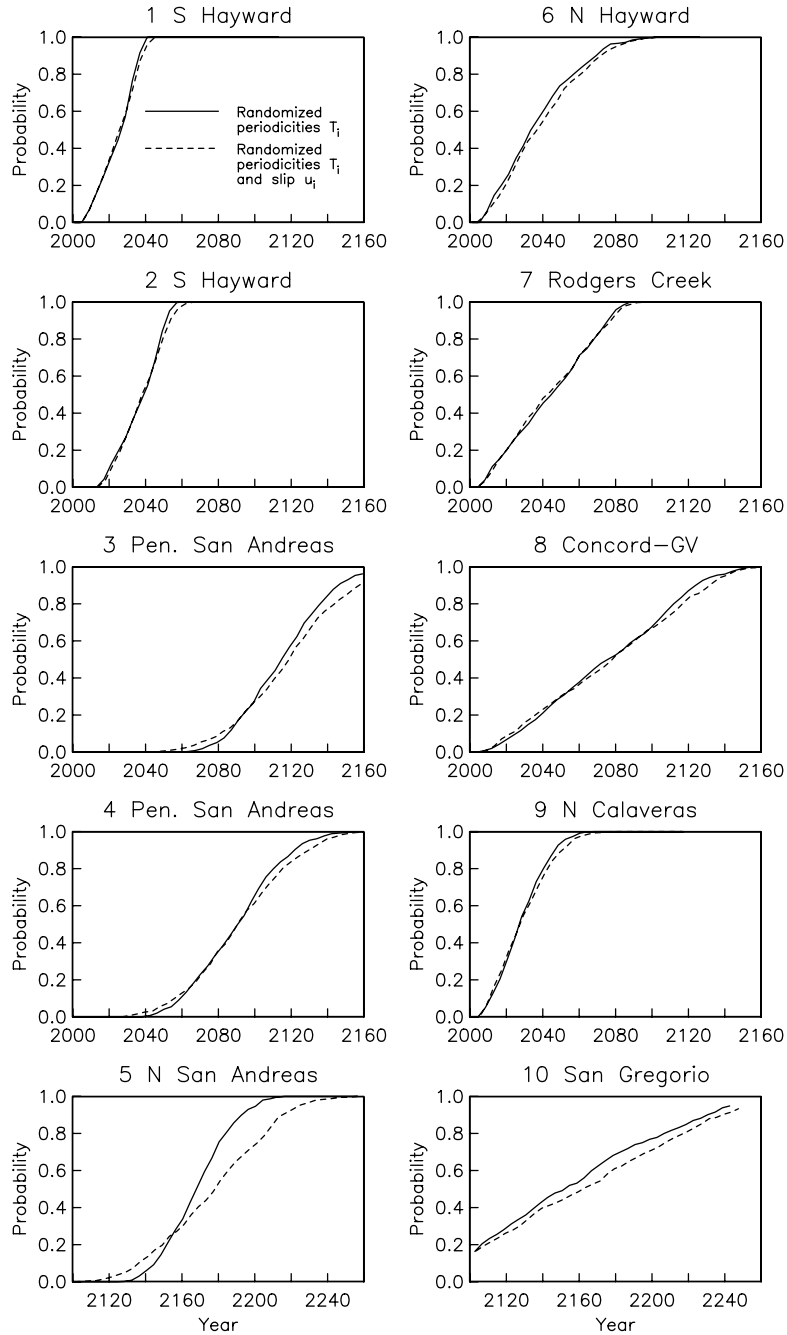


Figure 7. Cumulative probability of time to next rupture at 8 km depth along ten segments (identified in Figure 2) based on an identical Coulomb failure stress threshold between the penultimate event on each segment and the future rupture, combined with randomization of mean recurrence times $\{T_i\}$ along (solid curves) or randomization of mean recurrence times and slip distributions $\{u_i\}$ (dashed curves). The time of last rupture on the peninsular SAF is assigned the date 1838.

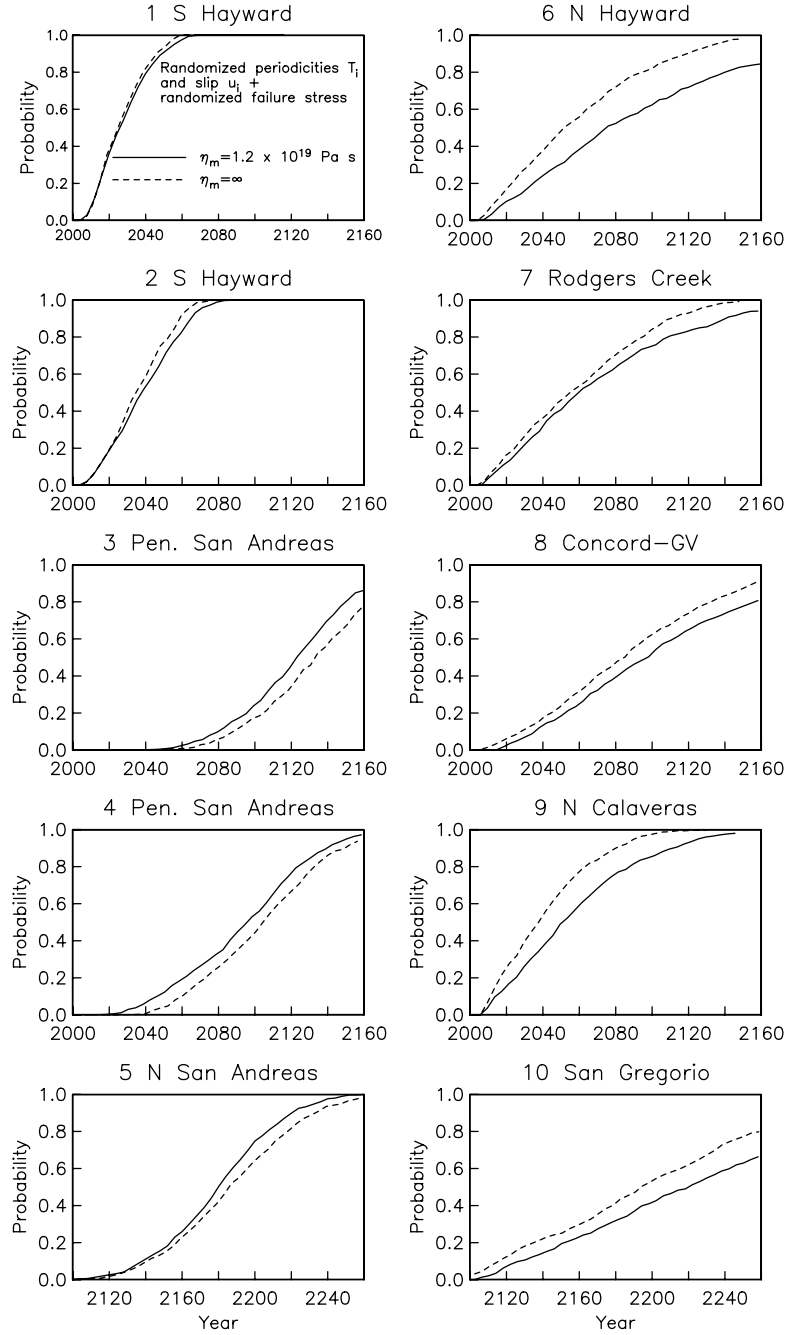


Figure 8. Cumulative probability of time to next rupture at 8 km depth along ten segments (identified in Figure 2) based on a randomized Coulomb failure stress threshold between the penultimate event on each segment and the future rupture, combined with randomization of mean recurrence times $\{T_i\}$, slip distributions $\{u_i\}$, and last event time t_i for pre-historic ruptures. Mantle viscosity η_m is either the value from *Pollitz and Nyst* [2004] (solid curves) or ∞ (dashed curves). The time of last rupture on the peninsular SAF is assigned the date 1838.

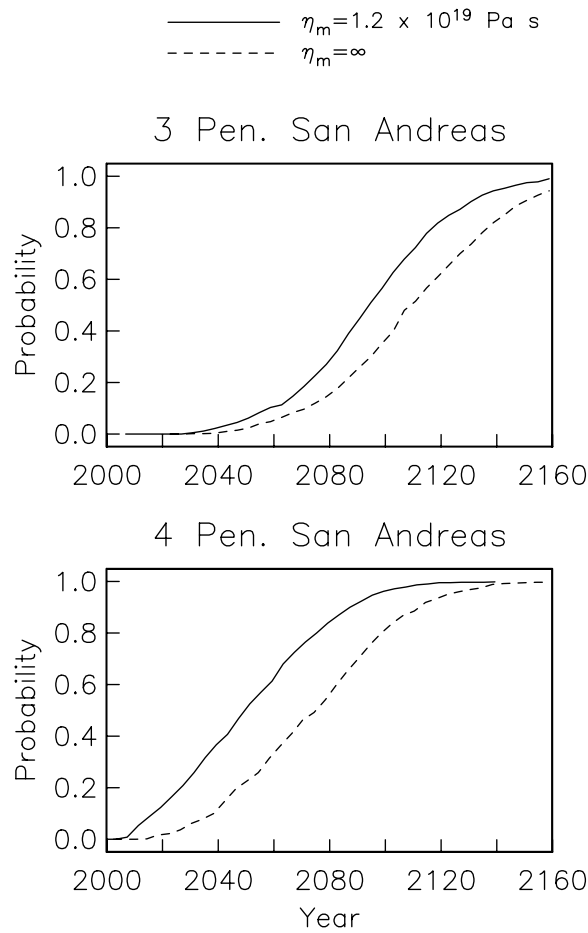


Figure 9. Same as Figure 6, except that the time of last rupture on the peninsular SAF is assigned the date 1906. Probability distributions for points on the peninsular SAF then refer to the time to return to the same stress state as existed just before 1906.

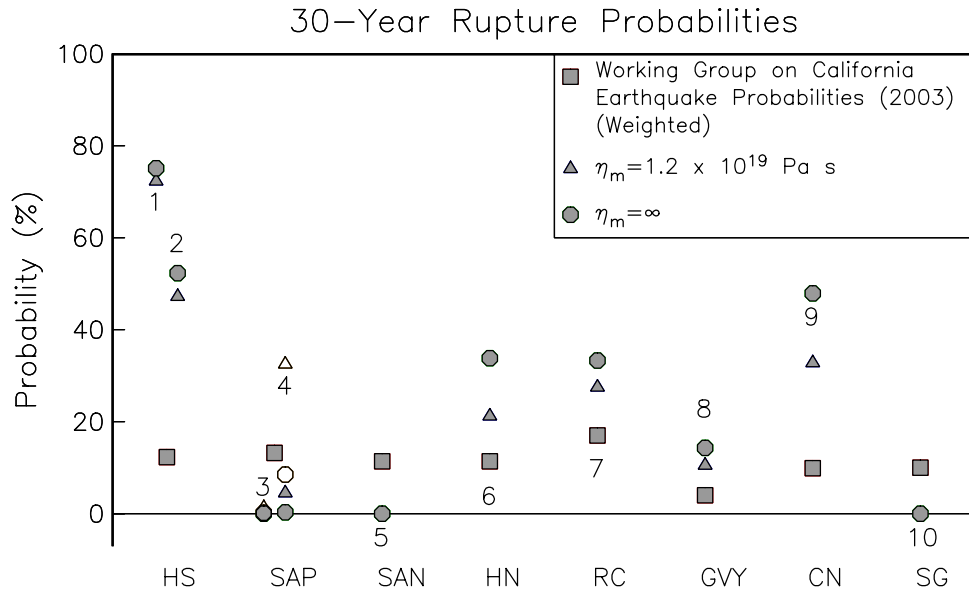


Figure 10. 30-year probabilities of rupture on selected segments. Squares are 2002-2032 magnitude ≥ 6.7 rupture probabilities from *Working Group on California Earthquake Probabilities* [2003]. (a) is weighted rupture probabilities from Table 6.1 (GVY and SG) or Table 6.3 (all other faults) of *Working Group on California Earthquake Probabilities* [2003]. (b) and (c) are, respectively, BPT-renewal and BPT-step rupture probabilities from Table 6.15 (GVY and SG) or Table 6.16 (all other faults) of *Working Group on California Earthquake Probabilities* [2003].

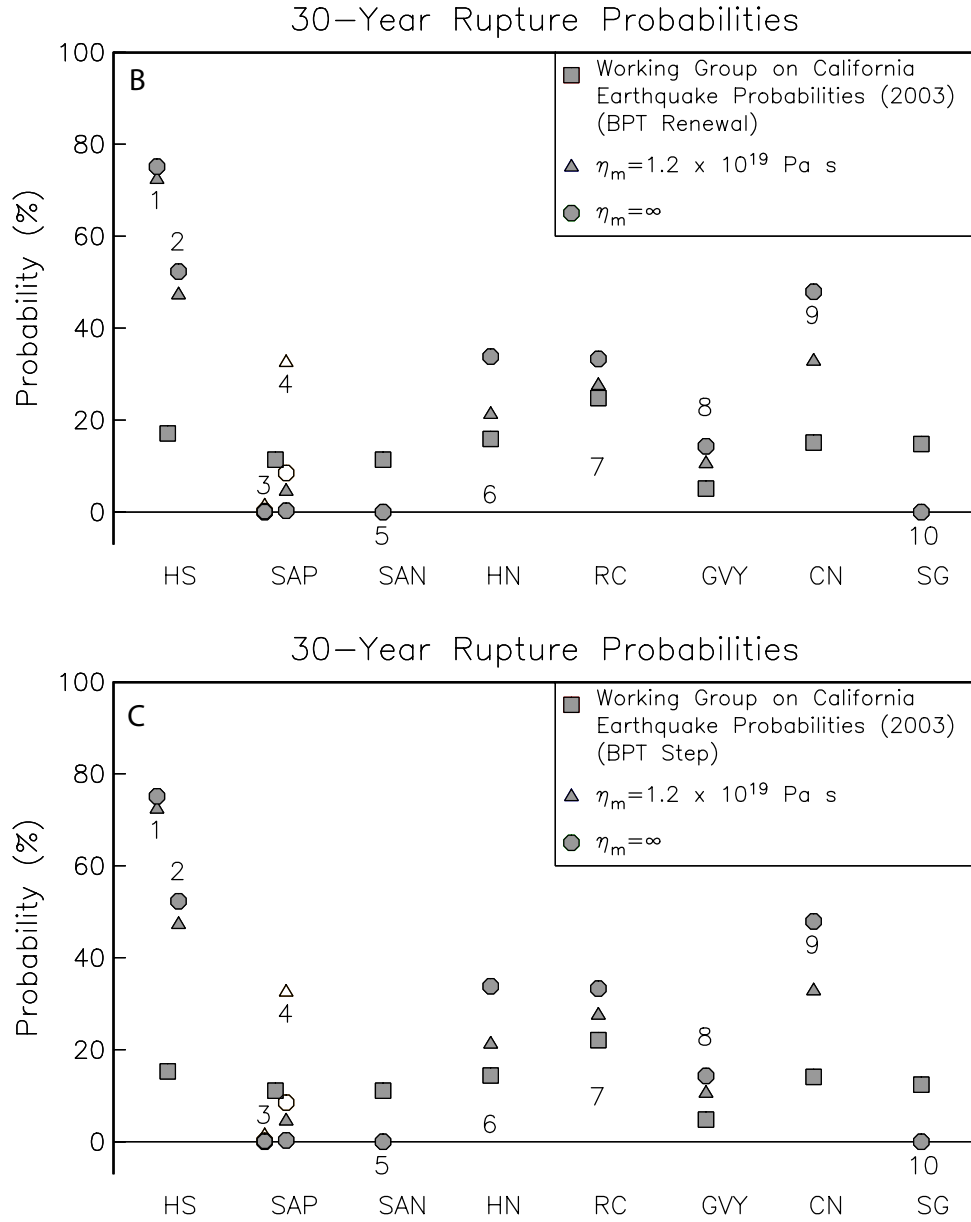


Figure 10. (continued) Triangles and squares are 2006-2036 rupture probabilities derived from Figure 9 for finite-viscosity and infinite-viscosity cases, respectively. Unfilled symbols denote the case of the SAP returning to its pre-1906 stress state (Figure 9). Numerals refer to fault locations in Figure 2.

Table 1. Fault geometry

Name	Type	d_u^\dagger (km)	d_l^\ddagger (km)	strike o	dip o	Length (km)	Ref.
Concord-GV	strike-slip*	0	15	340	90	60	1
N San Andreas	strike slip*	0	15	**	90	343	1
Rodgers Creek	strike-slip*	0	15	328	90	65	1
N Calaveras	strike-slip*	0	15	336	90	55	1
N Hayward	strike-slip*	5	15	329	90	37	1
S Hayward	strike slip*	5	15	326	90	40	4, 5
San Gregorio	strike-slip*	0	15	338	90	150	1
Peninsula	strike-slip*	0	15	324/312	90	71	1, 2, 3
San Andreas	strike slip*	0	15	**	90	473	1, 6
Loma Prieta	oblique slip	4.5	12.5	128	62	37	2, 7

* Pure right-lateral slip

** Variable strike towards NW

 \dagger Upper fault edge depth \ddagger Lower fault edge depth**Table 2.** Fault history

Name	t_i^{\S} Year	T_i^{\S} (years)	slip (m)	slip rate \star (mm/yr)	magnitude
Concord-GV	1700 (1685-1776)	400	1.8	4.5	7.10
N San Andreas	1720 (1695-1776)	400	3.0	7.5	7.60
Rodgers Creek	1740 (1690-1776)	300	3.0	10.0	7.27
N Calaveras	1760 (1670-1830)	300	1.5	5.0	7.02
N Hayward	1705 (1670-1776)	275	1.7	6.0	6.81
San Gregorio	1725 (1695-1776)	500	3.5	7.0	7.56
Peninsula	1838	200	1.2	6.0	7.12
S Hayward	1868	140	1.8	12.8	6.86
San Andreas	1906	400	2.3 - 8.6	5.8 - 21.5	7.98
Loma Prieta	1989	124	2.1	7.4 - 16.1	6.86

\S t_i and T_i are the date of last event and recurrence interval, respectively. Age range from Ref. 1 is given for pre-historic events.

\star Horizontal slip rate, equal to the characteristic slip divided by the recurrence interval.

(Listed slip rate is that associated with a particular earthquake cycle. Total slip rate on a segment, e.g., Peninsular San Andreas fault, is the sum of slip rates contributed by distinct cycles.)

¹ *Schwartz et al.*, 2006 [a]; ² *Bakun*, 1999 [a]; ³ *Pollitz et al.*, 2004 [a]; ⁴ *Yu and Segall*, 1996 [a];

⁵ *Lienkaemper et al.*, 2002 [a]; ⁶ *Thatcher et al.*, 1997 [a]; ⁷ *Marshall et al.*, 1991 [a]

Table 3. Fault slip rates

Name	seismic slip rate (mm/yr)	"seismogenic" creep* rate (mm/yr)	Total slip rate (mm/yr)	WGCEP [2003]† (mm/yr)
Concord-GV	4.5	3.0	7.5	2-8
San Andreas (38°N)	21.5	0.0	21.5	21-27
Rodgers Creek	10.0	0.0	10.0	7-11
N Calaveras	5.0	0.0	5.0	4-8
S Calaveras	0.0	16.0	16.0	12-18
N Hayward	6.0	4.0	10.0	7-11
S Hayward	12.8	0.0	12.8	7-11
San Gregorio	7.0	0.0	7.0	4-10
San Andreas (37°N)	14.6	0.0	14.6	13-21

* The creep rate at the depths where seismic slip also occurs, e.g. deeper than 5 km on the N and S Hayward faults.

† Slip rate 95% bounds from Table 3.8 of *Working Group on California Earthquake Probabilities* [2003].